International Journal of Bifurcation and Chaos, Vol. 13, No. 6 (2003) 1383–1422

RECENT DEVELOPMENTS IN CHAOTIC TIME SERIES ANALYSIS

YING-CHENG LAI
Department of Mathematics and Statistics,
Department of Electrical Engineering,
Arizona State University, Tempe, AZ 85287, USA

NONG YE
Department of Industrial Engineering,
Department of Computer Science and Engineering,
Arizona State University, Tempe, AZ 85287, USA

Received June 6, 2002

In this paper, two issues are addressed: (1) the applicability of the delay-coordinate embedding method to *transient* chaotic time series analysis, and (2) the Hilbert transform methodology for chaotic signal processing.

A common practice in chaotic time series analysis has been to reconstruct the phase space by utilizing the delay-coordinate embedding technique, and then to compute dynamical invariant quantities of interest such as unstable periodic orbits, the fractal dimension of the underlying chaotic set, and its Lyapunov spectrum. As a large body of literature exists on applying the technique to time series from chaotic attractors, a relatively unexplored issue is its applicability to dynamical systems that exhibit *transient chaos*. Our focus will be on the analysis of transient chaotic time series. We will argue and provide numerical support that the current delay-coordinate embedding techniques for extracting unstable periodic orbits, for estimating the fractal dimension, and for computing the Lyapunov exponents can be readily adapted to transient chaotic time series.

A technique that is gaining an increasing attention is the Hilbert transform method for signal processing in nonlinear systems. The general goal of the Hilbert method is to assess the spectrum of the instantaneous frequency associated with the underlying dynamical process. To obtain physically meaningful results, it is necessary for the signal to possess a proper rotational structure in the complex plane of the analytic signal constructed by the original signal and its Hilbert transform. We will describe a recent decomposition procedure for this task and apply the technique to chaotic signals. We will also provide an example to demonstrate that the methodology can be useful for addressing some fundamental problems in chaotic dynamics.

Keywords: Chaotic time series; delay coordinates; embedding; transient chaos; correlation dimension; Lyapunov exponents; unstable periodic orbits; Hiebert transform; instantaneous frequency.

1. Introduction

Parallel to the rapid development of nonlinear dynamics since the late seventies, there has been a tremendous amount of effort on data analysis. Suppose an experiment is conducted and some time series are measured. Such a time series can be, for instance, a voltage signal from a physical or biological experiment, or the concentration of a substance in a chemical reaction, or the EEG signals from a

patient with epileptic seizures, or the amount of instantaneous traffic at a point in the internet, and so on. The general question is: what can we say about the underlying dynamical system that generates the time series, if the equations governing the time evolution of the system are unknown and the only available information about the system is the measured time series?

This paper reviews two approaches in nonlinear data analysis: (1) the delay-coordinate embedding technique [Takens, 1981], and (2) the time-frequency method based on the Hilbert transform [Huang *et al.*, 1998]. The embedding method has been proven useful, particularly for time series from low-dimensional, deterministic or mostly deterministic[1] dynamical systems. That is, for situations where the dynamical invariant set responsible for the behavior of the measured time series is low-dimensional and the influence of noise is relatively small, the delay-coordinate embedding method can yield reliable information essential for understanding the underlying dynamical system. The method has been applied to many disciplines of science and engineering [Abarbanel, 1996; Kantz & Schreiber, 1997], and it is also the key to controlling chaos [Ott *et al.*, 1990; Garfinkel *et al.*, 1992; Schiff *et al.*, 1994; Boccaletti *et al.*, 2000], one of the most fruitful areas in applicable chaotic dynamics in the last decade [Chen, 1999].

The mathematical foundation of the delay-coordinate embedding technique was laid by Takens in his seminal paper [Takens, 1981]. He proved that, under fairly general conditions, the underlying dynamical system can be faithfully reconstructed from time series in the sense that, a one-to-one correspondence can be established between the reconstructed and the true but unknown dynamical systems. Based on the reconstruction, quantities of importance for understanding the system can be estimated, such as the relative weights of determinisicity and stochasticity embedded in the time series, the dimensionality of the underlying dynamical system, the degree of sensitivity on initial conditions as characterized by the Lyapunov exponents, and unstable periodic orbits that constitute the skeleton of the invariant set responsible for the observed dynamics.

There exists a large body of literature on the application of the delay-coordinate embedding technique to dynamical systems with chaotic attractors [Abarbanel, 1996; Kantz & Schreiber, 1997]. Time series obtained from such a system can in principle be as long as one wishes. Another common situation of interest is where the dynamical system exhibits only transient chaos [Grebogi *et al.*, 1982, 1983; Grassberger & Kantz, 1985; Tél, 1990, 1996]. For such a system, a measured signal exhibits a random behavior during an initial time interval before finally settling into a nonchaotic state. The conventional wisdom may be simply to disregard the transient portion of the data and to concentrate on the final state. By doing this, however, information about the system may be lost, because the irregular part of the data may contain important hints about the system dynamics. Transient chaos is in fact ubiquitous in dynamical systems. In view of this, analyzing transient chaotic time series is as important as analyzing sustained chaotic data, yet to our knowledge, the problem has begun to be addressed only recently [Janosi & Tél, 1994; Dhamala *et al.*, 2000, 2001].

It has been known that the dynamical invariant sets responsible for transient chaos are nonattracting chaotic saddles [Grebogi *et al.*, 1982, 1983; Grassberger & Kantz, 1985; Tél, 1990, 1996]. Here, "nonattracting" means that a trajectory starting from a typical initial condition in a phase-space region containing the saddle stays near the saddle for a finite amount of time exhibiting chaotic behavior, exits the region, and approaches asymptotically to a final state. Chaotic saddles are common in nonlinear dynamical systems. For instance, a chaotic saddle can arise after a chaotic attractor is destroyed at crisis [Grebogi *et al.*, 1982, 1983]. Or, a saddle can be found in *every* periodic window where it coexists with a periodic attractor. Physically, chaotic saddles lead to observable phenomena such as chaotic scattering [Tél & Ott, 1993], fractal basin boundaries [McDonald *et al.*, 1985], fractal concentrations of passive particles advected in open hydrodynamical flows [Jones & Aref, 1988; Jones *et al.*, 1989; Young & Jones, 1991; Jung & Ziemniak, 1992; Jung *et al.*, 1993; Ziemniak *et al.*, 1994; Péntek *et al.*, 1995; Stolovitzky *et al.*, 1995; Karolyi & Tél, 1997], and fractal distribution of chemicals in environmental flows [Toroczkai *et al.*, 1998; Károlyi *et al.*, 1999; Nishikawa *et al.*, 2002]. Mathematically, chaotic

[1]In realistic situations environmental noise is inevitable. Here "mostly deterministic" means that the system evolves according to a set of determinsitic rules, under the influence of small noise.

saddles are closed, bounded, and invariant sets with dense orbits. They are the "soul" of chaotic dynamics [Smale, 1967].

One focus of this paper will then be on analyzing time series from transient chaotic systems. The following problems will be addressed: (1) detecting unstable periodic orbits, (2) estimating the correlation dimension, and (3) computing the Lyapunov exponents. The main point is that, despite the difficulty in dealing with a transient chaotic system for which the chaotic phases containing the essential information about the system are short, many of the standard algorithms that are used to estimate dynamical quantities from time series of sustained chaotic processes can be applied to ensembles of transient chaotic time series. It is not necessary to construct a single long time series from a set of shorter ones. All that is required is a collection of transient time series, starting from different initial conditions. Section 2 is devoted to the essential features of the delay-coordinate embedding technique and various methods for computing the dynamical invariants from transient chaotic time series.

The Hilbert-transform based time-frequency method [Huang *et al.*, 1998] can be applied to nonlinear and/or nonstationary time series. The technique can in principle be applied to random and nonstationary time series, and it can be useful if one is interested in analyzing the system in terms of the distribution of the instantaneous, physical frequencies.[2] In certain circumstances the time-frequency method can be powerful for identifying the physical mechanisms responsible for the characteristics of the instantaneous-frequency spectrum of the data [Huang *et al.*, 1998].

The time-frequency method to be described in this paper aims to extract the fundamental physical frequencies from chaotic time series. Roughly, a random but bounded time series implies recurrence in time of the measured physical quantity. The recurrence can be regarded, conceptually, as being composed of rotations in a physical or mathematical space. The questions are: how many principal rotations exist and what are the frequency characteristics of these rotations? The recent groundbreaking idea by Huang *et al.* [1998] leads to a powerful technique that provides answers to these questions. It should be stressed here that the frequency components here correspond to rotations and, hence, they are different from these in the traditional Fourier analysis or in the wavelet analysis. In many situations the instantaneous frequencies of the rotations contain much more information than the Fourier or wavelet frequency components that are associated with simple mathematical functions such as the harmonics. The instantaneous frequencies of rotations can thus be physically more meaningful. While Fourier and wavelet analyses are well developed methods for signal processing in linear systems, Huang *et al.* argue that the Hilbert analysis is fundamentally superior to both the Fourier and wavelet analyses for nonstationary and nonlinear time series [Huang *et al.*, 1998]. Section 3 will detail concepts such as rotations and instantaneous frequencies, analytic signals, and the Hilbert transform, describe the corresponding decomposition technique developed by Huang *et al.* [1998], and illustrate that the methodology can be applied to chaotic systems. For completeness, at the beginning of Sec. 3, we briefly review the Fourier spectral and wavelet methods.

2. Embedding Method for Chaotic Time Series Analysis

2.1. *Reconstruction of phase space*

Let $u_i(t)$ $(i = 1, \ldots, l)$ be a set of l measurements. In principle, the measured time series come from an underlying dynamical system that evolves the state variable in time according to a set of deterministic rules, which are generally represented by a set of differential equations, with or without the influence of noise. Mathematically, any such set of differential equations can be easily converted to a set of first-order, autonomous equations. The dynamical variables from all the first-order equations constitute the *phase space*, and the number of such variables is the *dimension* of the phase space, which we denote by M. The phase-space dimension can in general be quite large. For instance, in a fluid experiment, the governing equation is the Navier–Stokes equation which is a nonlinear partial differential equation. In order to represent the system by first-order ordinary differential equations via, say, the procedure of spatial discretization, the number of required equations is infinite. The phase-space-dimension in this case is thus infinite.

[2]These are not the traditional Fourier frequencies.

However, it often occurs that the asymptotic evolution of the system lives on a dynamical invariant set of only finite dimension. The assumption here is that the details of the system equations in the phase space and of the asymptotic invariant set that determines what can be observed through experimental probes, are unknown. The task is to estimate, *based solely on one or few time series*, practically useful statistical quantities characterizing the invariant set, such as its dimension, its dynamical skeleton, and its degree of sensitivity on initial conditions. The delay-coordinate embedding technique established by Takens [1981] provides a practical solution to this task [Packard *et al.*, 1980]. In particular, Takens' embedding theorem guarantees that a topological equivalence of the phase space of the intrinsic unknown dynamical system can be reconstructed from time series, based on which characteristics of the dynamical invariant set can be estimated.

Takens' delay-coordinate embedding method goes, as follows. From each measured time series $u_i(t)$ $(i = 1, \ldots, l)$, the following vector quantity of q components is constructed,

$$\mathbf{u}_i(t) = \{u_i(t),\, u_i(t+\tau), \ldots,\, u_i[t+(q-1)\tau]\}\,,$$

where τ is the *delay time*. Since there are l time series, a vector with $m \equiv ql$ components can be constructed, as follows:

$$\begin{aligned}\mathbf{x}(t) &= \{\mathbf{u}_1(t),\, \mathbf{u}_2(t), \ldots,\, \mathbf{u}_l(t)\} \\ &= \{u_1(t),\, u_1(t+\tau), \ldots,\, u_1[t+(q-1)\tau]\,, \\ &\quad u_2(t),\, u_2(t+\tau), \ldots,\, u_2[t+(q-1)\tau], \ldots, \\ &\quad u_l(t),\, u_l(t+\tau), \ldots,\, u_l[t+(q-1)\tau]\}\,, \quad (1)\end{aligned}$$

where m is the embedding dimension. Clearly, the delay time τ and the embedding dimension m are the two fundamental parameters in the delay-coordinate embedding method.

1. *Delay time* τ. In order for the time-delayed components $u_i(t + j\tau)$ $(j = 1, \ldots, q-1)$ to serve as independent variables, the delay time τ needs to be chosen carefully. Roughly, if τ is too small, then adjacent components $u_i(t)$ and $u_i(t+\tau)$ will be too correlated for them to serve as independent coordinates. If, on the other hand, τ is too large, then neighboring components are too uncorrelated for the purpose. Empirically, one can examine the autocorrelation function of $u_i(t)$ and decide a proper delay time [Theiler, 1986]. In particular, one computes

$$c(T) \equiv \frac{\langle u_i(t) u_i(t+T)\rangle}{\langle u_i^2(t)\rangle}\,,$$

where $\langle\cdot\rangle$ stands for time average. The delay time τ can be chosen to be the value of T such that $c(T)/c(0) \approx e^{-1}$.

There exist various alternative empirical methods for choosing a proper delay time [Liebert & Schuster, 1989; Liebert *et al.*, 1991; Buzug & Pfister, 1992; Kember & Fowler, 1993; Rosenstein *et al.*, 1994], which all yield similar results. A firmer theoretical foundation may be possible by exploring the statistics for testing continuity and differentiability from chaotic time series proposed by Pecora *et al.* [Pecora *et al.*, 1995; Pecora & Carroll, 1996; Pecora *et al.*, 1997; Pecora & Carroll, 2000; Goodridge *et al.*, 2001].

2. *Embedding dimension* m. In order to have a faithful representation of the true dynamical system, the embedding dimension m should be sufficiently large. Takens' theorem [Takens, 1981] provides a lower bound for m. In particular, suppose the dynamical invariant set lies in a d-dimensional manifold (or subspace) in the phase space. Then, if $m > 2d$, the m-dimensional reconstructed vectors $\mathbf{x}(t)$ have a one-to-one correspondence to the vectors of the true dynamical system. This result can be understood by the following simple mathematical argument. Consider two smooth surfaces of dimensions d_1 and d_2 in an M-dimensional space and examine the set of their intersections. The question is whether they intersect generically in the sense that the intersections cannot be removed by small perturbations to either surface. The natural approach is then to look at the dimension d_I of the intersecting set, which is

$$d_I = d_1 + d_2 - M\,.$$

If $d_I \geq 0$, the intersection is generic. For example, consider the intersection of two one-dimensional curves in a two-dimensional plane: $d_1 = d_2 = 1$ and $M = 2$. We obtain: $d_I = 0$, which means that the intersecting set consists of points, and the intersections are generic because small perturbations cannot remove them. If, however, $M = 3$, then $d_I < 0$, which means that two one-dimensional curves do not intersect generically in a three-dimensional space. These two cases, together with an additional one ($d_1 = 1$, $d_2 = 2$, and $M = 3$), are illustrated in Fig. 1. For the case of embedding, we can ask

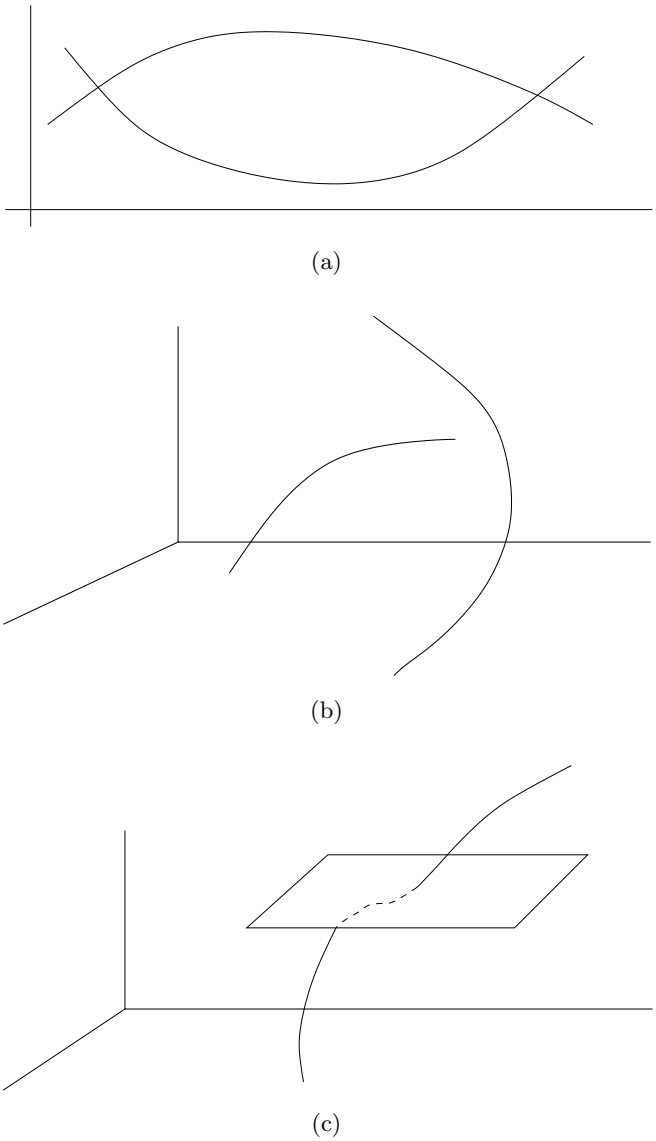

Fig. 1. Illustration of generic and nongeneric intersections of simple geometric sets: (a) $d_1 = d_2 = 1$ and $M = 2$ (generic intersection), (b) $d_1 = d_2 = 1$ and $M = 3$ (nongeneric intersection), and (c) $d_1 = 1$, $d_2 = 2$, and $M = 3$ (generic intersection).

whether the dynamical invariant set would intersect itself in the reconstructed phase space. In order to obtain a one-to-one correspondence between points on the invariant sets in the actual and reconstructed phase spaces, self-intersection must not occur. Thus, taking $d_1 = d_2 = d$ and $M = m$, no self-intersection requires $d_I < 0$, which means that $m > 2d$.

While Takens' theorem assumes that the relevant dimension d of the set is that of the manifold in which the set lies, this dimension can be quite different from the dimension of the set itself, which is physically more relevant. The work by Sauer, Yorke, and Casdagli [Sauer *et al.*, 1991] extends Takens's theorem to relax the dimension requirement: the dimension d can in fact be the box-counting dimension D_0 [Farmer *et al.*, 1983] of the invariant set.

2.2. *Detection of unstable periodic orbits*

A fundamental feature that differs a deterministic chaotic system from a stochastic one is the existence of an infinite number of unstable periodic orbits which constitute the skeleton of the chaotic invariant set [Auerbach *et al.*, 1987; Gunaratne & Procaccia, 1987; Morita *et al.*, 1987; Grebogi *et al.*, 1988; Biham & Wenzel, 1989; Lai *et al.*, 1997; Lai, 1997; Zoldi & Greenside, 1998; Davidchack *et al.*, 2000]. Computation of unstable periodic orbits from system equations [Biham & Wenzel, 1989; Schmelcher & Diakonos, 1997, 1998; Schmelcher *et al.*, 1998; Davidchack & Lai, 1999; Davidchack *et al.*, 2001; Pingel *et al.*, 2001] and their detection from experimental time series have been an active area of research [Lathrop & Kostelich, 1989; Mindlin *et al.*, 1990; Pawelzik & Schuster, 1991; Badii *et al.*, 1994; Pierson & Moss, 1995; Christini & Collins, 1995; Pei & Moss, 1996a, 1996b; So *et al.*, 1996, 1997; Allie & Mees, 1997; Dhamala *et al.*, 2000, 2001]. At a fundamental level, unstable periodic orbits embedded in a chaotic invariant set are related to its natural measure [Grebogi *et al.*, 1988; Lai *et al.*, 1997; Lai, 1997], which is the base for defining physically important quantities such as the fractal dimensions and Lyapunov exponents. At a practical level, successful detection of unstable periodic orbits indicates the deterministic origin of the underlying dynamical process. In what follows, we will review the basic concepts of the natural measure and unstable periodic orbits, describe an algorithm for their detection from chaotic time series, and provide numerical examples.

2.2.1. *The natural measure: why are unstable periodic orbits important?*

One of the most important problems in dealing with a chaotic system is to compute long term statistics such as averages of physical quantities, Lyapunov exponents, dimensions, and other invariants of the probability density or the measure. The interest in

the statistics roots in the fact that trajectories of deterministic chaotic systems are apparently random and ergodic. These statistical quantities, however, are *physically meaningful* only when the measure being considered is the one generated by a typical trajectory in the phase space. This measure is called the natural measure and it is invariant under the evolution of the dynamics [Grebogi *et al.*, 1988].

The importance of the natural measure can be assessed by examining how trajectories behave in a chaotic system. Due to ergodicity, trajectories on a chaotic set exhibit sensitive dependence on initial conditions. Moreover, the long-time probability distribution generated by a typical trajectory on the chaotic set is generally highly singular.[3] For a chaotic attractor, a trajectory originated from a random initial condition in the basin of attraction visits different parts of the attractor with drastically different probabilities. Call regions with high probabilities "hot" spots and regions with low probabilities "cold" spots. Such hot and cold spots in the attractor can in general be interwoven on arbitrarily fine scales. In this sense, chaotic attractors are said to possess a multifractal structure. Due to this singular behavior, one utilizes the concept of the natural measure to characterize chaotic attractors [Ott, 1993]. To obtain the natural measure, one covers the chaotic attractor with a grid of cells and examine the frequencies with which a typical trajectory visits these cells in the limit that both the length of the trajectory goes to infinity and the size of the grid goes to zero [Farmer *et al.*, 1983]. Except for an initial condition set of Lebesgue measure zero in the basin of attraction, these frequencies in the cells are the natural measure. Specifically, let $f(\mathbf{x}_0, T, \varepsilon_i)$ be the amount of time that a trajectory from a random initial condition $\mathbf{x}_0$ in the basin of attraction spends in the ith covering cell C_i of edge length ε_i in a time T. The probability measure of the attractor in the cell C_i is

$$\mu_i = \lim_{\varepsilon_i \to 0} \lim_{T \to \infty} \frac{f(\mathbf{x}_0, T, \varepsilon_i)}{T} . \tag{2}$$

The measure is called *natural* if it is the same for all randomly chosen initial conditions, that is, for all initial conditions in the basin of attraction except for a set of Lebesgue measure zero. The spectrum of an infinite number of fractal dimensions quantifies the behavior of the natural measure for multifractal chaotic attractors [Grassberger & Procaccia, 1983a].

The above description can be seen by considering a physical example, the forced damped pendulum

$$\begin{aligned} \frac{dx}{dt} &= y \,, \\ \frac{dy}{dt} &= -0.05y - \sin\, x + 2.5\, \sin\, t \,. \end{aligned} \tag{3}$$

Figure 2(a) plots [Lai, 1997], on the stroboscopic surface of section defined at discrete times $t_n = 2\pi n$, $n = 1, \ldots$, a trajectory of 1.5×10^5 points on the chaotic attractor, where the abscissa and the ordinate are the angle $x(t_n)$ and the angular velocity $y(t_n) \equiv dx/dt|_{t_n}$ of the pendulum, respectively. Figure 2(b) shows the one-dimensional probability distribution on the attractor at $y = -2$. To obtain Fig. 2(b), a one-dimensional array of 1000 rectangular cells is defined in the x-direction at $y = -2$. The frequency of visits to each cell is then computed by utilizing a trajectory of 10^7 points on the surface of section. In fact, probability distributions on any line intersecting the chaotic attractor exhibit similar behavior. These results suggest a highly singular probability distribution on the chaotic attractor.

Because of the physical importance of the natural measure, it is desirable be able to understand and characterize it in terms of the fundamental dynamical quantities of the chaotic set. There is nothing more fundamental than to express the natural measure in terms of the periodic orbits embedded in a chaotic attractor.

A chaotic set has embedded within itself an infinite number of unstable periodic orbits. These periodic orbits are *atypical* in the sense that they form a Lebesgue measure zero set. With probability one, randomly chosen initial conditions do not yield trajectories which live on unstable periodic orbits. Invariant measures produced by unstable periodic orbits are thus atypical, and there is an infinite number of such atypical invariant measures embedded in a chaotic attractor. The "hot" and "cold" spots are a reflection of these atypical measures. The natural measure, on the other hand, is typical in the sense that it is generated by a trajectory originated from any one of the randomly chosen initial

[3]Take, for example, the logistic map $x_{n+1} = 3.8x_n(1 - x_n)$ that exhibits a chaotic attractor. A simple argument [Ott, 1993] based on mapping of the probability in a small interval suggests that singularities in the probability distribution occurs at all forward images of the critical point $x_c = 1/2$ under the map, which are dense in the attractor.

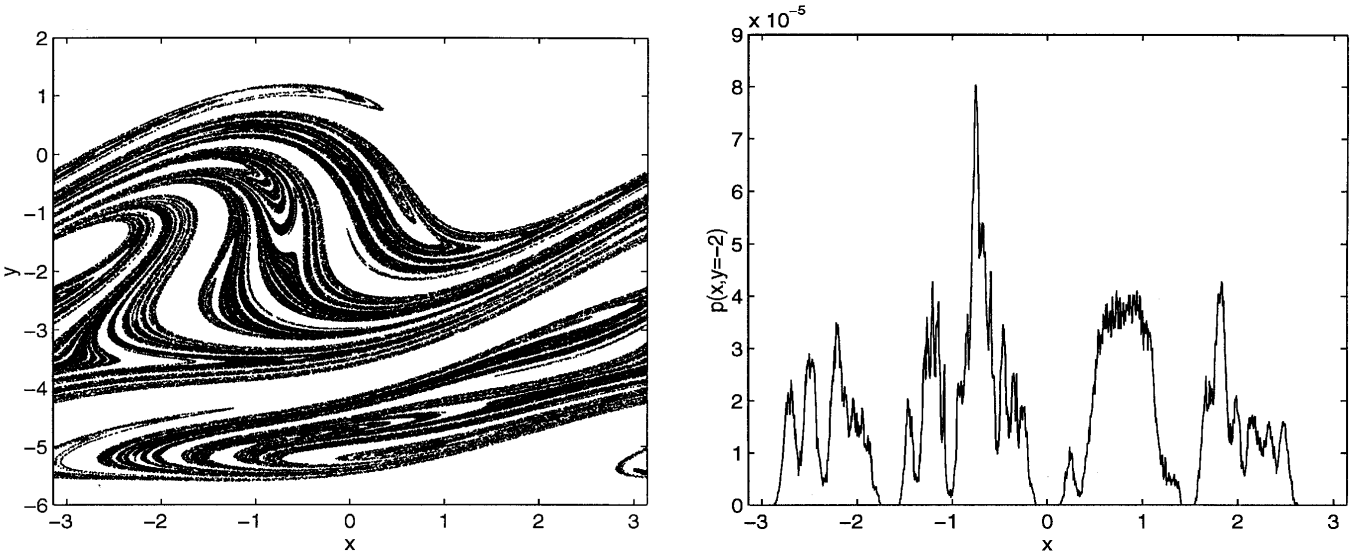

(a) (b)

Fig. 2. For the forced damped pendulum system Eq. (3), (a) a trajectory of 1.5×10^5 points on the chaotic attractor on the stroboscopic surface of section, and (b) the distribution of the natural measure in a one-dimensional array of 1000 rectangular cells in the x-direction at $y = 2$. The size of each cell is $2\pi/1000 \times 0.06$. Numerically, the total measure contained in the attractor is normalized to unity. Apparently, the natural measure is singular.

conditions in the basin of attraction. A typical trajectory visits a fixed neighborhood of any one of the periodic orbits from time to time. Thus, chaos can be considered as being organized with respect to the unstable periodic orbits [Auerbach *et al.*, 1987; Gunaratne & Procaccia, 1987].

Grebogi, Ott, and Yorke derived [Grebogi *et al.*, 1988], for the special case of hyperbolic chaotic systems,[4] a formula relating the natural measure of the chaotic set in the phase space to the expanding eigenvalues of all the periodic orbits embedded in the set. Specifically, consider an N-dimensional map $\mathbf{M}(\mathbf{x})$. Let $\mathbf{x}_{ip}$ be the ith fixed point of the p-times iterated map, i.e. $\mathbf{M}^p(\mathbf{x}_{ip}) = \mathbf{x}_{ip}$. Thus each $\mathbf{x}_{ip}$ is on a periodic orbit whose period is either p or a factor of p. The natural measure of a chaotic attractor in a phase-space region S is given by

$$\mu(S) = \lim_{p\to\infty} \sum_{\mathbf{x}_{ip}\in S} \frac{1}{L_1(\mathbf{x}_{ip}, p)}\,, \qquad (4)$$

where $L_1(\mathbf{x}_{ip}, p)$ is the magnitude of the expanding eigenvalue of the Jacobian matrix $\mathbf{DM}^p(\mathbf{x}_{ip})$, and the summation is taken over all fixed points of $\mathbf{M}^p(\mathbf{x})$ in S. This formula can be derived under the assumption that the phase space can be divided into cells via a Markov partition, a condition that is generally satisfied by hyperbolic chaotic systems. Explicit verification of this formula was done for several analyzable hyperbolic maps [Grebogi *et al.*, 1988]. Equation (4) is theoretically significant and interesting because it provides a fundamental link between the natural measure and various atypical invariant measures embedded in a chaotic attractor. The applicability of Eq. (4) to nonhyperbolic chaotic systems has also been addressed recently [Lai *et al.*, 1997; Lai, 1997].

2.2.2. *Extracting unstable periodic orbits from transient chaotic time series*

A powerful algorithm for detecting unstable periodic orbits from chaotic time series is due to Lathrop and Kostelich (LK) [Lathrop & Kostelich, 1989]. The method is based on identifying sets of

[4]The dynamics is hyperbolic on a chaotic set if at each point of the trajectory the phase space can be split into an expanding and a contracting subspaces and the angle between them is bounded away from zero. Furthermore, the expanding subspace evolves into the expanding one along the trajectory and the same is true for the contracting subspace. Otherwise the set is nonhyperbolic. In general, nonhyperbolicity is a complicating feature because it can cause fundamental difficulties in the study of the chaotic systems, such as the shadowability of numerical trajectories by true trajectories [Hammel *et al.*, 1987, 1988; Grebogi *et al.*, 1990; Dawson *et al.*, 1994; Lai *et al.*, 1999a; Lai & Grebogi, 1999; Lai *et al.*, 1999b].

recurrent points in the reconstructed phase space. To do this, one first reconstructs a phase-space trajectory $\mathbf{x}(t)$ from a measured scalar time series $\{u(t)\}$ by using the delay-coordinate embedding method described in Sec. 2.1. To identify unstable periodic orbits, one follows the images of $\mathbf{x}(t)$ under the dynamics until a value $t_1 > t$ is found such that $\|\mathbf{x}(t_1) - \mathbf{x}(t)\| < \varepsilon$, where ε is a prespecified small number that defines the size of the recurrent neighborhood at $\mathbf{x}(t)$. In this case, $\mathbf{x}(t)$ is called an (T, ε) recurrent point, and $T = t_1 - t$ is the *recurrence time*. A recurrent point is not necessarily a component of a periodic orbit of period T. However, if a particular recurrence time T appears frequently in the reconstructed phase space, it is likely that the corresponding recurrent points are close to periodic orbits of period T. The idea is then to construct a histogram of the recurrence times and identify peaks in the histogram. Points that occur frequently are taken to be, approximately, components of the periodic orbits. The LK-algorithm has been used to detect unstable periodic orbits, for instance, from measurements of a chaotic chemical reaction [Lathrop & Kostelich, 1989].

More recently, the LK algorithm has been adapted to detecting unstable periodic orbits from short, transiently chaotic series [Dhamala *et al.*, 2000]. The reason that the LK-algorithm is applicable to transient time series lies in the statistical nature of this method, as a histogram of recurrence times can be obtained even with short time series. Provided that there is a large number of such time series so that a good statistics of the recurrence times can be obtained, unstable periodic orbits embedded in the underlying chaotic set can be identified. It is not necessary to concatenate many short time series to form a single long one (such concatenations are invariably problematic [Janosi & Tél, 1994]). Intuitively, since the time series are short, periodic orbits of short periods can be detected.

To demonstrate the LK-algorithm, here we take the numerical examples reported in [Dhamala *et al.*, 2000] with the following chaotic Rössler system [Rössler, 1976]:

$$\begin{aligned} \frac{dx}{dt} &= -y - z\,, \\ \frac{dy}{dt} &= x + ay\,, \\ \frac{dz}{dt} &= b + (x - c)z\,, \end{aligned} \tag{5}$$

where a, b, and c are parameters. There is transient chaos when the set of parameter values yields a periodic window in which a stable periodic attractor and a chaotic saddle coexist. For instance, for $a = b = 0.2$ and $c = 5.3$, the system falls in a periodic window of period 3. Typical measurement of a dynamical variable, say $x(t)$, exhibits chaotic behavior for a finite amount of time before settling in the period-3 attractor. In [Dhamala *et al.*, 2000], 10 such time series are generated by integrating the Rössler system from different initial conditions, and the corresponding time series $x(t)$ for $0 \le t \le 4$ are recorded. The lifetime of the chaotic transient is about 4. These time series are assumed to be the only available information about the system. For each time series, a seven-dimensional vector space is reconstructed by using the delay time $\tau = 0.02$. To obtain recurrence times, it is necessary to determine ε, the size of the recurrent neighborhood. The value of ε must not be large to avoid too many false positives, but ε must not be so small that genuine recurrences are missed. Typically, it is found in numerical experiments that the number of recurrences $N(\varepsilon)$ increases with the length and the number of the individual transient trajectories, and with ε. It tends to saturate when ε is too large. The value of ε at which $N(\varepsilon)$ saturates is taken to be an appropriate size of the recurrent neighborhood. For the Rössler system, $\varepsilon = 2\%$ of the root-mean-square (rms) value of the chaotic signal is used [Dhamala *et al.*, 2000]. Figure 3(a) shows the histogram of the recurrence times for the 10 transient chaotic time series from the period-3 window. Figures 3(b)–3(d) show, in the plane of $x(t)$ versus $x(t + \tau)$, three recurrent orbits. The orbit in Fig. 3(b) has the shortest recurrence time, so it is a "period-1" orbit. Figures 3(c) and 3(d) show a period-3 and a period-8 orbits, respectively. The orbits are selected from the set of recurrent points comprising the corresponding peak in the histogram. In general, it is found [Dhamala *et al.*, 2000] that the LK-algorithm is capable of yielding many periodic orbits of low periods.

In an experimental setting, time series are contaminated by dynamical and/or observational noise. A question is whether periodic orbits can still be extracted from noisy transient chaotic time series. Qualitatively, under the influence of noise, the effective volume of recurrent region in the

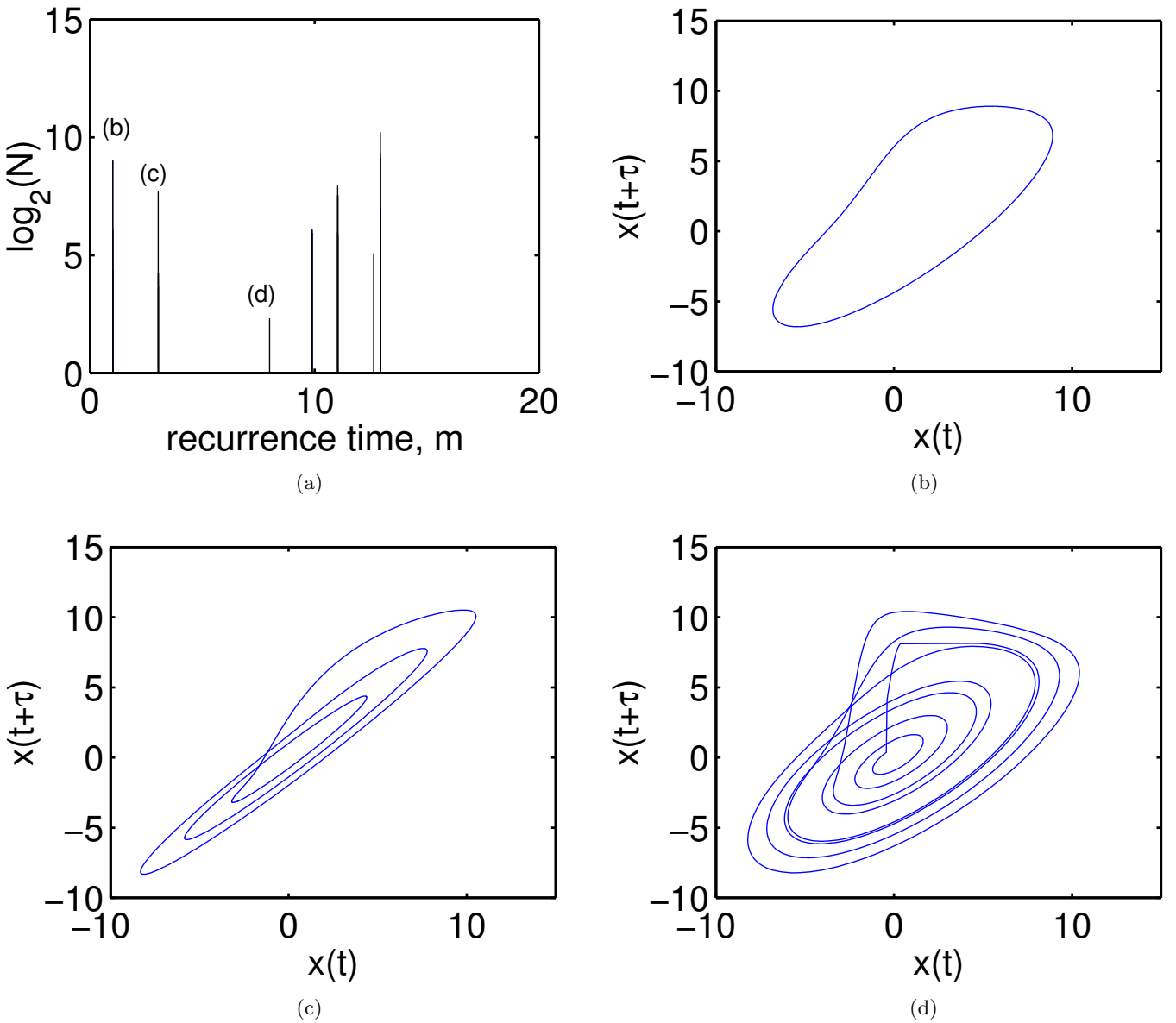

Fig. 3. For the Rössler system: (a) histogram of the recurrence time T, (b–d) a period-1, a period-3, and a period-8 recurrent orbits extracted from the histogram in (a), respectively.

phase space decreases and, hence, a decrease in the number of recurrences is expected. Figures 4(a)–4(d) show the number of recurrent points (a) and three periodic orbits extracted from 10 transient chaotic time series with additive noise of the form $G(0, 0.01)$, a normal (Gaussian) distribution centered at 0 with variance 0.01. This noise level represents a rms value that is approximately 0.5% of that of the chaotic signal. It can be seen that at this low noise level, periodic orbits can still be reliably detected. It is found, however, that for the Rössler system at $\varepsilon = 2\%$ of the rms value of the chaotic signal with noise beyond 1%, no periodic orbits can be extracted from the histogram of recurrences. One way to assess the influence of noise is to compute, at several fixed values of ε, how the number of recurrent points decreases as the noise amplitude (η) is increased. Figures 5(a) and 5(b) show the result of such computations for (a) $\varepsilon = 2\%$ and (b) $\varepsilon = 6\%$ of the rms value of the signal. It can be seen that the number of recurrent points goes to zero at $\eta \approx \varepsilon/2$, which can be understood, as follows. Under noise of amplitude η, both the center and the boundary of the recurrent region are uncertain within η. Thus, the effective phase-space volume in d dimensions in which two points can still be considered within

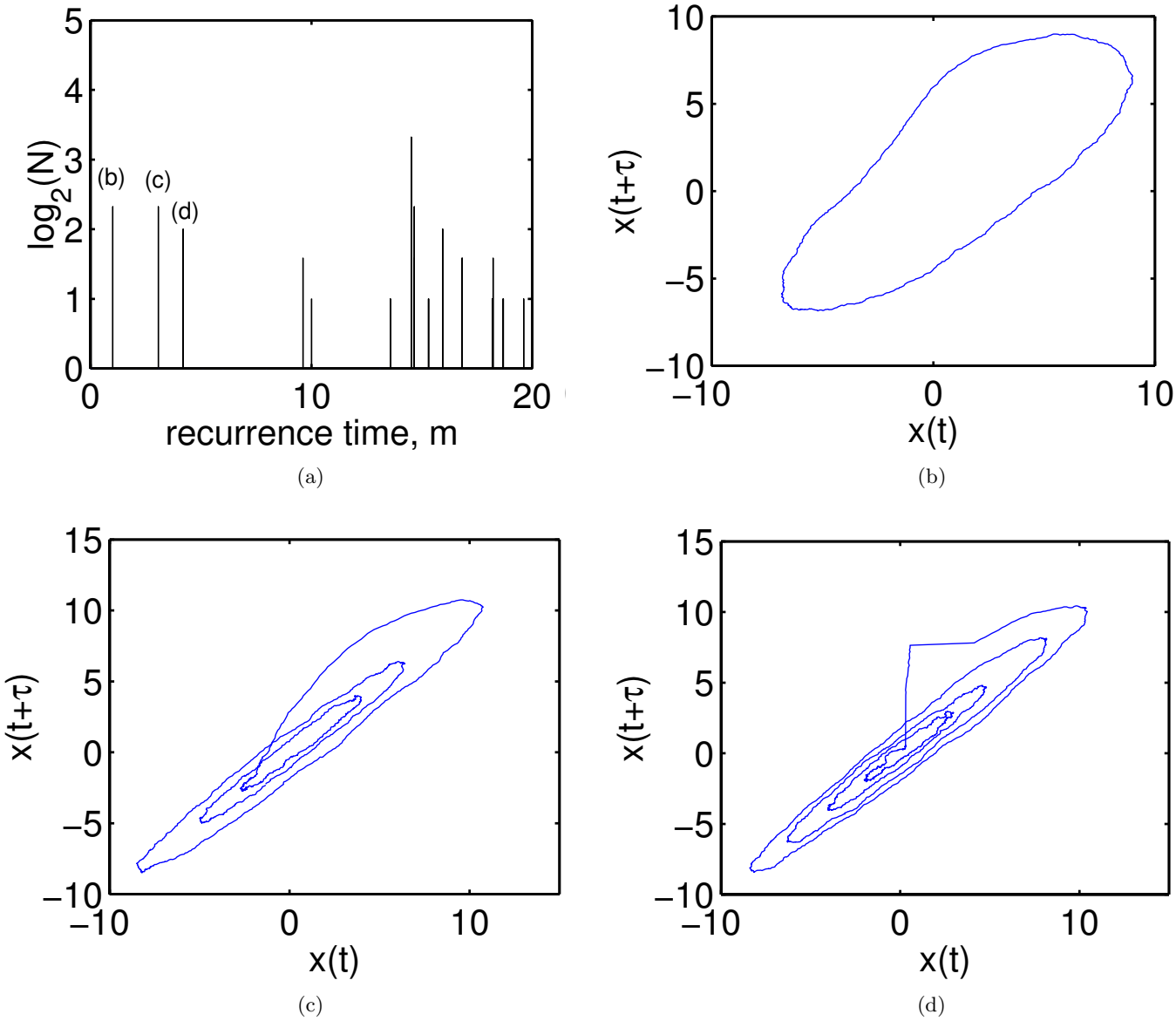

Fig. 4. For a noisy Rössler system: (a) histogram of the recurrence time T, (b–d) a period-1, a period-2, and a period-4 recurrent orbits extracted from the histogram in (a), respectively, where $\varepsilon = 6\%$ and the rms value of the noise is at about 0.5% of that of the chaotic signal.

distance ε (recurrent) is proportional to $(\varepsilon-\eta)^d-\eta^d$, which vanishes at $\eta = \varepsilon/2$. Since ε should be small to guarantee recurrence, we see that the tolerable noise level is also small.

2.2.3. *Detectability of unstable periodic orbits from transient chaotic time series*

An issue of interest concerns the detectability of unstable periodic orbits from chaotic time series [Pei *et al.*, 1998]. This is particularly relevant for transient chaos because trajectories on a chaotic saddle have an average lifetime time τ staying near the saddle and, hence, it is difficult for a typical trajectory to contain periodic orbits of period larger than τ. Effort may then be devoted to connect short time series so that the resulting long time series would contain periodic orbits of larger period [Janosi & Tél, 1994]. Such a task may be difficult. If one fails to detect periodic orbits of high periods, the question is whether one should attempt to increase the number of measurements so that more time series are available. Or, one may attempt

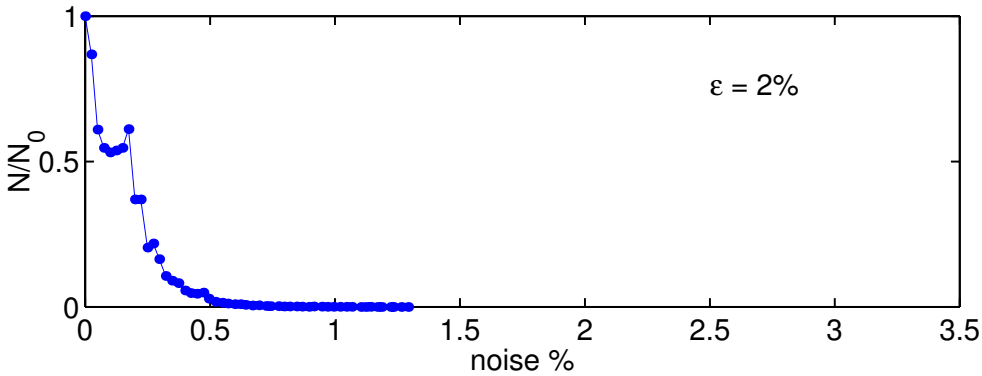

(a)

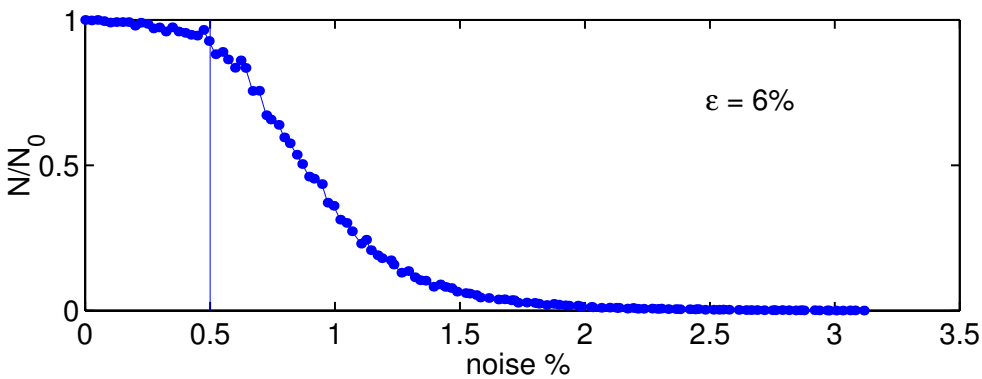

(b)

Fig. 5. For the noisy Rössler system, the relative number (N/N_0) of recurrent points versus the amplitude of noise for two values of the size of the recurrent neighborhood: (a) $\varepsilon = 2\%$ and (b) $\varepsilon = 6\%$ of the rms value of the signal, where N_0 is the number of recurrent points at zero amplitude of noise. The vertical line in (b) denotes the noise level at which periodic orbits in Fig. 4 are extracted.

to improve techniques to link these time series, a computationally demanding task because it is essentially a problem of optimizing many time series and the computation required in any optimization problem typically increases greatly as the number of elements involved is increased. The main point is that in detecting unstable periodic orbits from transient chaos, the probability of detecting orbits of higher periods is typically exponentially small [Dhamala *et al.*, 2000, 2001]. This is an *intrinsic* dynamical property of the underlying chaotic saddle and, hence, increasing the number of measurements or improving techniques of detection will not help enhance the chance to detect these orbits.

Let $\Phi(p)$ be the probability to detect any period-p orbit. A scaling relation for $\Phi(p)$ can be derived [Dhamala *et al.*, 2000, 2001] by noting that $\Phi(p)$ is actually the probability for a trajectory to stay in a small neighborhood of any periodic orbit of period p. For a trajectory to stay in an ν-neighborhood of all p points of the ith orbit of period p, the trajectory must come within $\delta = \nu e^{-\lambda_i(p)p}$ of any of the p points when it first encounters with the periodic orbit, where $\lambda_i(p) > 0$ is the Lyapunov exponent of this orbit. The probability for this event is $\phi_i(p) \sim \delta^{D_i}$, where D_i is the pointwise dimension of any one of the p points of this periodic orbit. The exponential factor $e^{-\lambda_i(p)p}$ is proportional to the natural measure associated with this periodic orbit [Grebogi, *et al.*, 1988]. The probability $\Phi(p)$ is the accumulative probability of all $\phi_i(p)$,

$$\Phi(p) = \sum_{i=1}^{K(p)} \phi_i(p) \sim \sum_{i=1}^{K(p)} \nu^{D_i} \exp\left[-\lambda_i(p) D_i p\right], \quad (6)$$

where $K(p)$ is the total number of periodic points of period p. Since $\lambda_i(p)$ and D_i are the local positive Lyapunov exponent and pointwise dimension of periodic orbits of period p, for large p, we

expect them to obey distributions centered at λ_1 and D_1, respectively, where λ_1 and D_1 are the positive Lyapunov exponent and the information dimension of the chaotic saddle. Thus, the main dependence of $\Phi(p)$ on p is

$$\Phi(p) \sim e^{-\lambda_1 D_1 p} K(p) \sim e^{(-\lambda_1 D_1 + h_T)p} = e^{-\gamma p}\,, \quad (7)$$

where γ is the exponential scaling exponent and h_T is the topological entropy. The Kaplan–Yorke formula can be used for chaotic saddles [Hsu *et al.*, 1988; Hunt *et al.*, 1996] to express D_1 in terms of the Lyapunov exponents $\lambda_2 < 0 < \lambda_1$ and the lifetime τ,

$$D_1 = (\lambda_1 - 1/\tau)(1/\lambda_1 + 1/|\lambda_2|)\,,$$

which yields the following scaling exponent:

$$\gamma = \lambda_1 - h_T + \frac{\lambda_1^2}{|\lambda_2|} - \frac{1}{\tau}\left(1 + \frac{\lambda_1}{|\lambda_2|}\right). \quad (8)$$

Equations (7) and (8) are applicable to chaotic saddles in two-dimensional invertible maps or in three-dimensional flows. Note that for chaotic attractors ($\tau \to \infty$), we have for the scaling exponent: $\gamma \approx \lambda_1 - h_T + \lambda_1^2/|\lambda_2|$.

To test Eqs. (7) and (8) numerically, Dhamala *et al.* use the Hénon map [Hénon, 1976]

$$\begin{aligned} x_{n+1} &= a - x_n^2 + b y_n\,, \\ y_{n+1} &= x_n\,, \end{aligned} \quad (9)$$

where a and b are parameters, as unstable periodic orbits in the chaotic saddles of the map can be computed systematically [Biham & Wenzel, 1989]. For the following set of three parameter values: $a = 1.6$, 1.8, and 2.0, there is transient chaos [Lai *et al.*, 1993]. Representative chaotic saddles for $a = 1.6$ and $a = 1.8$ are shown in Figs. 6(a) and 6(b), respectively, which are obtained by the procedure in [Nusse & Yorke, 1989]. For each value of a, 10^6 initial conditions are chosen in the region $[-2, 2] \times [-2, 2]$ containing the chaotic saddle, which yield 10^6 transient time series [Dhamala *et al.*, 2000]. For a given period p, the fractions of times that these 10^6 time series get close to every periodic orbit of period p can be computed. These fractions are used to yield an estimated value for the probability $\Phi(p)$, which increases with the number of transient time series and also with the length of the individual trajectories. Figures 7(a)–7(d) show $\ln \Phi(p)$ versus p for $a = 1.6$, 1.8, and 2.0, respectively. These plots indicate behavior of exponential decay, and the decay exponents are given by the slopes of the plots. To compute the theoretical scaling exponents in Eq. (8), it is necessary to compute the Lyapunov exponents, the topological entropy, and the lifetime of the chaotic saddles. The following techniques are used in the computation [Dhamala *et al.*, 2000,

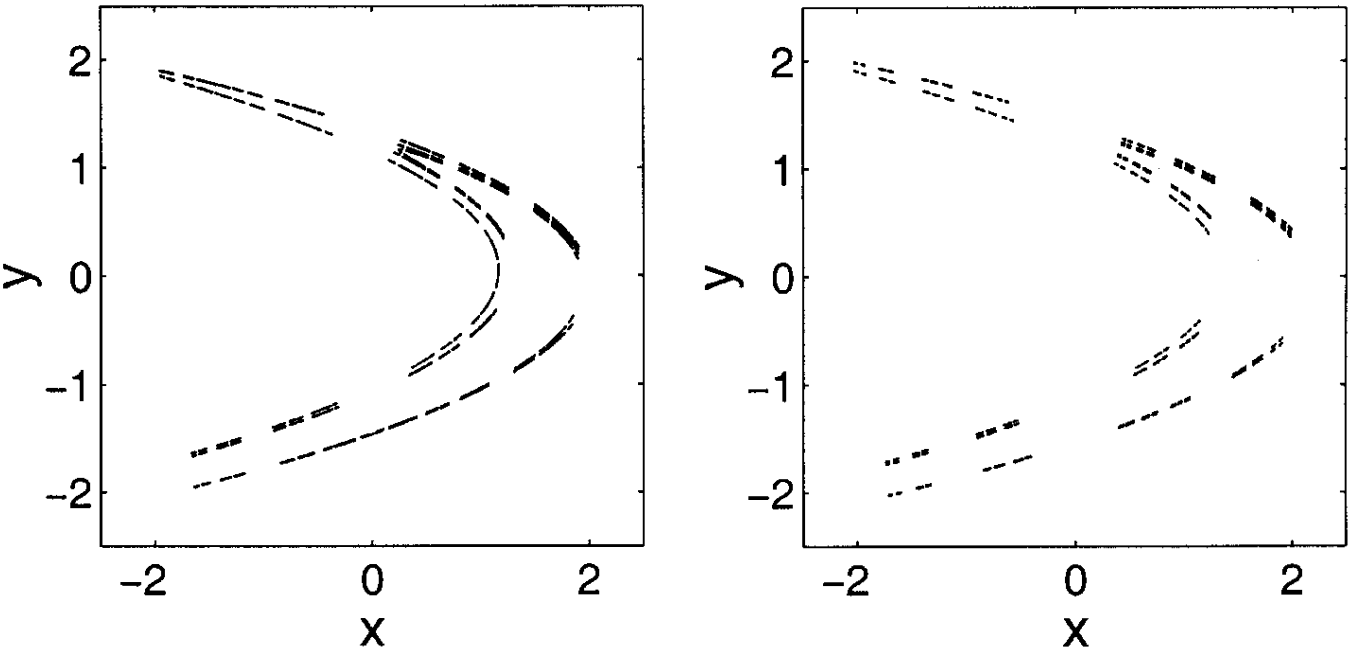

(a) $a = 1.6$ (b) $a = 1.8$

Fig. 6. Chaotic saddles of the Hénon map for (a) $a = 1.6$ and (b) $a = 1.8$.

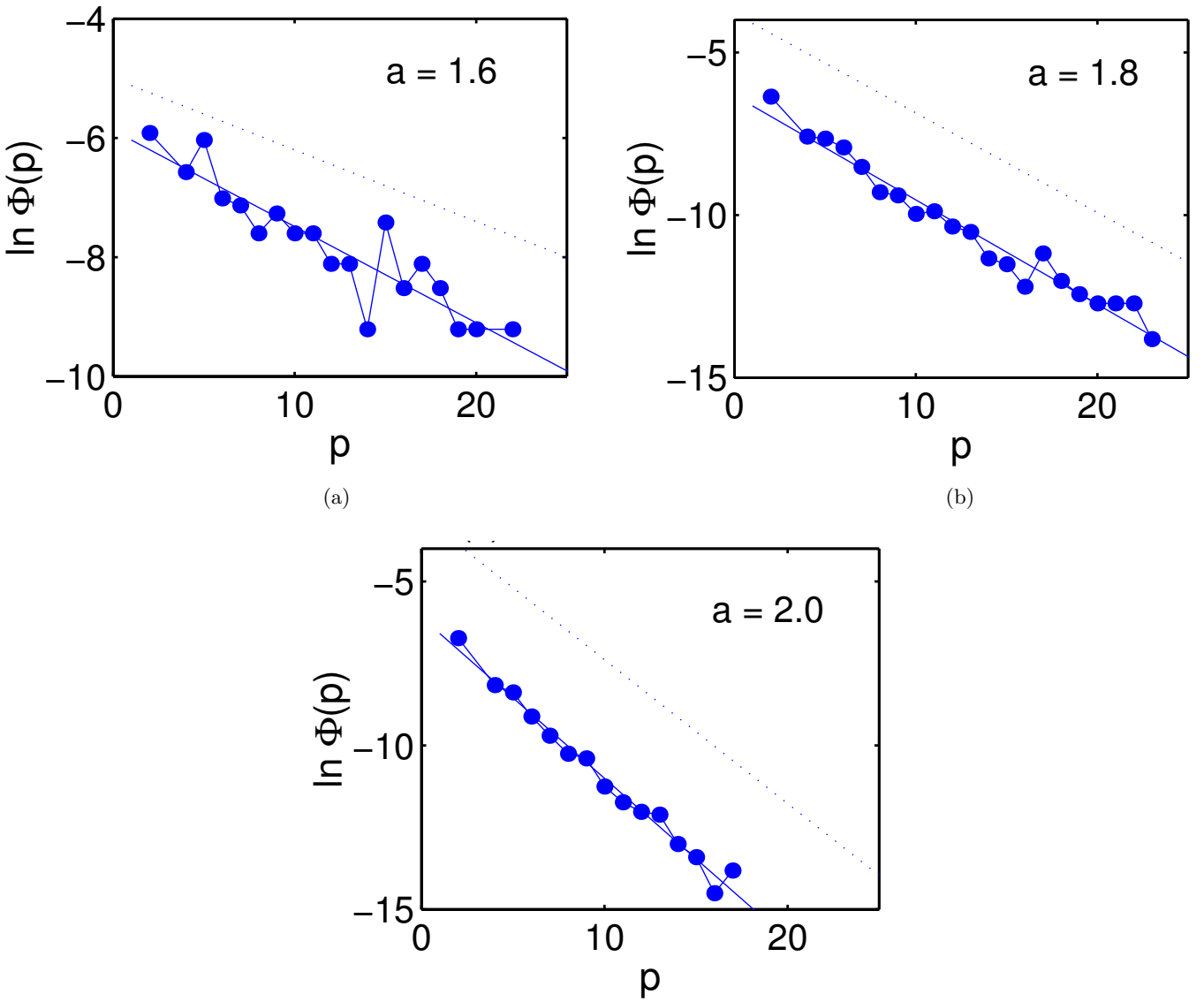

Fig. 7. (a–c) For the Hénon map at $a = 1.6$, 1.8, and 2.0, $\ln \Phi(p)$ versus p. The dotted lines indicate the theoretically predicted slopes of $\ln \Phi(p)$ versus p.

2001]: (1) the procedure to obtain a long trajectory on the chaotic saddle [Nusse & Yorke, 1989; Jacobs *et al.*, 1997] from which the Lyapunov exponents can be computed; (2) the method by Chen *et al.* [1991] to compute the topological entropy; and (3) the sprinkler method to compute τ [Hsu *et al.*, 1988]. The slopes of the dashed straight lines in Figs. 7(a)–7(d) are the theoretical slopes for the corresponding chaotic saddles. The numerical slopes appear to agree reasonably well with the theoretical ones, as shown further in Table 1, where the numerical and theoretical slopes, together with the values of other quantities involved in Eq. (8), are listed.

2.3. *Computation of dimension*

2.3.1. *Basics*

An often computed dimension in nonlinear time series analysis is the correlation dimension D_2, which is a good approximation of the box-counting dimension D_0: $D_2 \leq D_0$. Grassberger and Procaccia show in their seminal contribution [Grassberger & Procaccia, 1983b] that D_2 can be evaluated by using the correlation integral $C(\varepsilon)$, which is the probability that a pair of points, chosen randomly in the reconstructed phase space, is separated by a distance less than ε. Let N be the number of points in the

Table 1. Theoretical and numerical values of the scaling exponent γ at four different parameters for the Hénon map.

a	λ_1	λ_2	h_T	τ	γ(theoretical)	γ(numerical)
1.6	0.58	−1.78	0.53	11.2	0.12	0.13 ± 0.04
1.8	0.81	−2.01	0.54	4.7	0.31	0.32 ± 0.03
2.0	0.87	−2.07	0.53	5.4	0.44	0.47 ± 0.04

reconstructed vector time series $\mathbf{x}(t)$. The correlation integral can be approximated by the following sum,

$$C_N(\varepsilon) = \frac{2}{N(N-1)} \sum_{j=1}^{N} \sum_{i=j+1}^{N} \Theta(\varepsilon - |\mathbf{x}_i - \mathbf{x}_j|), \quad (10)$$

where $\Theta(\cdot)$ is the Heaviside function: $\Theta(x) = 1$ for $x \geq 0$ and 0 otherwise, and $|\mathbf{x}_i - \mathbf{x}_j|$ stands for the distance between points $\mathbf{x}_i$ and $\mathbf{x}_j$. Grassberger and Procaccia argue that the correlation dimension is given by [Grassberger & Procaccia, 1983b]

$$D_2 = \lim_{\varepsilon \to 0} \lim_{N \to \infty} \frac{\log C_N(\varepsilon)}{\log \varepsilon}. \quad (11)$$

In practice, for a time series of finite length, the sum in Eq. (10) also depends on the embedding dimension m. Due to such dependencies, the correlation dimension D_2 is usually estimated by examining the slope of the linear portion of the plot of $\log C_N(\varepsilon)$ versus $\log \varepsilon$ for a series of increasing values of m. For $m < D_2$, the dimension of the reconstructed phase space is not high enough to resolve the structure of the dynamical state and, hence, the slope approximates the embedding dimension. As m increases, the resolution of the dynamical state in the reconstructed phase space is improved. Typically, the slope in the plot of $\log C_N(\varepsilon)$ versus $\log \varepsilon$ increases with m until it reaches a plateau; its value at the plateau is then taken as the estimate of D_2 [Grassberger & Procaccia, 1983b; Ding *et al.*, 1993]. For an infinite and noiseless time series, the value of m at which this plateau begins to satisfy is $m = \text{Ceil}(D_2)$, where $\text{Ceil}(D_2)$ is the smallest integer greater than or equal to D_2 [Ding *et al.*, 1993]. In a realistic situation, short data sets and observational noise can cause the plateau onset to occur at a value of m which can be larger than $\text{Ceil}(D_2)$. Even so, the embedding dimension at which the plateau is reached still provides a reasonably sharp upper bound for the true correlation dimension D_2. Dependencies of the length of the linear scaling region on fundamental parameters such as m, τ, and $m\tau$ have been analyzed systematically in [Lai *et al.*, 1996; Lai & Lerner, 1998].

These points can be seen by utilizing the Hénon map Eq. (9) at the standard parameter values $a = 1.4$ and $b = 0.3$. The map is believed to possess a chaotic attractor, as shown in Fig. 8(a) in the two-dimensional phase space (x, y). A typical time series $\{x_n\}$ is shown in Fig. 8(b). The theoretical value of the correlation dimension of the chaotic attractor is $D_2 \approx 1.2$ [Lai *et al.*, 1996; Lai & Lerner, 1998].

The GP-algorithm can be applied to estimating the correlation dimension from the time series $\{x_n\}$. To select the delay time τ, note that any discrete-time map can be regarded as arising from a Poincaré surface of section of a continuous-time flow [Ott, 1993]. Thus, one iteration of the map corresponds to roughly one period of oscillation of the continuous-time signal $x(t)$, which, for chaotic systems, is approximately the decay time of the autocorrelation of $x(t)$. As an empirical rule, the delay time can be chosen to be $\tau = 1$ for chaotic time series from discrete-time maps. Equivalently, for chaotic signal $x(t)$ from a continuous-time flow, the delay time should be chosen approximately as the average period of oscillation.

After the delay time τ is chosen, the next step is to compute the correlation integral $C_N(\varepsilon)$ for a set of systematically increasing values of the embedding dimension m. Figure 9 shows, for $N = 2 \times 10^4$, the plots of $C_N(\varepsilon)$ versus ε on the base-2 logarithmic scale for $m = 1, \ldots, 8$. The lines are approximately linear, and they are parallel for $m \geq 2$. Least-squares fits give $D_2 \approx 1.2$ for $m \geq 2$, indicating that the correlation dimension can be estimated reliably from a time series by utilizing the GP-algorithm. The saturation of the slope occurs at $m = 2$, which is the smallest integer above the value of D_2. Recall that the embedding theorem requires a minimum embedding dimension of $2D_0 + 1$, which is 4 for the Hénon chaotic attractor. This is because the task here is to estimate the dimension only, while the embedding theorem guarantees a one-to-one correspondence between the reconstructed and the true chaotic attractors. A dimension estimate does not necessarily require such a one-to-one correspondence. For instance, consider a two-dimensional surface in a three-dimensional space. The projection of this surface onto a two-dimensional plane is still a two-dimensional region. Thus, its dimension can be estimated even in a two-dimensional subspace.

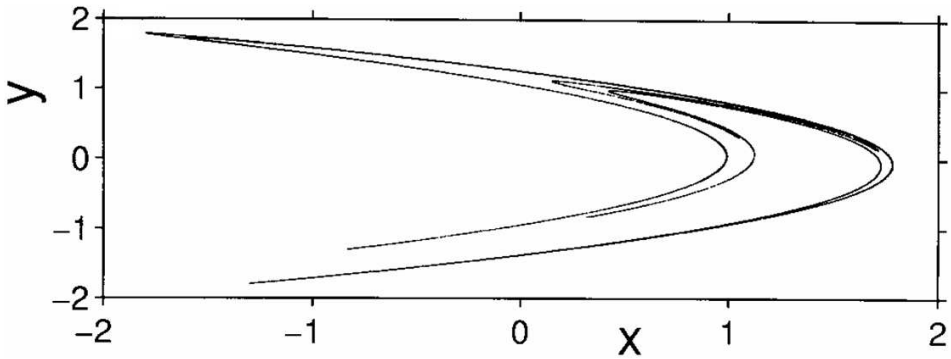

(a)

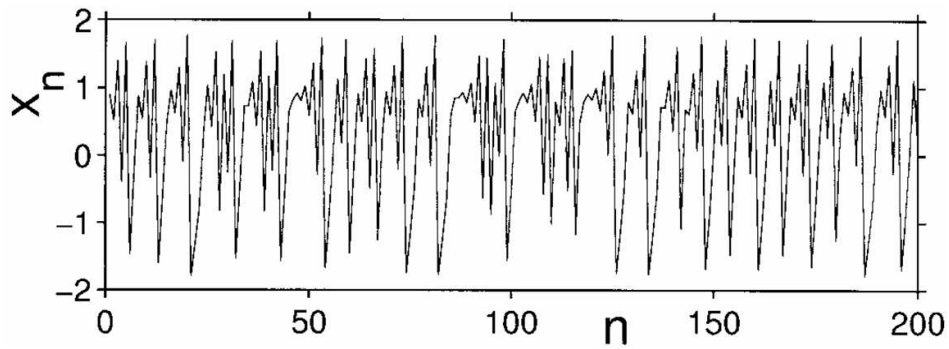

(b)

Fig. 8. (a) The Hénon chaotic attractor and (b) a typical chaotic time series.

2.3.2. *Applicability of GP algorithm to transient chaotic time series*

An important question is whether the GP paradigm [Eqs. (10) and (11)] is applicable to transient time series from chaotic saddles. Recently, an argument is provided which appears to give an affirmative answer to this question [Dhamala *et al.*, 2001].

To derive the GP-algorithm for transient chaotic time series, it is necessary to define the natural measure associated with a nonattracting chaotic saddle. Imagine a phase-space region S that contains such a saddle. If a large number N_0 of random initial conditions is distributed in S, the corresponding trajectories will leave S eventually as time progresses. They do so by being attracted along the stable manifold, wandering near the chaotic saddle, and then exiting along the unstable manifold. Let $N(n)$ be the number of trajectories that still remain in S at time n. For large n, $N(n)$ decreases exponentially due to the chaotic but nonattracting nature of the saddle[5]

$$N(n) = N_0 e^{-n/\tau}\,, \tag{12}$$

where τ is the average lifetime of the trajectories on the chaotic saddle.

The nonattracting nature of the chaotic saddle renders more complicated the definition of its natural measure as compared with that for a chaotic attractor. Because of the invariance of the natural measure under the dynamics, it is necessary in the definition to compensate for the escape of chaotic

[5]Exponential decay of the number of trajectories near the chaotic saddle is characteristic of transient chaos in dissipative dynamical systems. In particular, say we sprinkle a large number N_0 of initial conditions in a phase-space region containing the chaotic saddle and compute $N(t)$, the number of trajectories still remaining in the region at time t. Then one typically finds that $N(t)$ decays exponentially with time [Grebogi *et al.*, 1983; Grassberger & Kantz, 1985; Tél, 1990]. For simple one-dimensional maps such as the following piecewise linear one on the unit interval: $x_{n+1} = 2\eta x_n$ if $0 \le x_n < 1/2$ and $x_{n+1} = 2\eta(x_n - 1) + 1$ if $1/2 < x \le 1$, where $\eta > 1$, it can be argued easily that there is a chaotic saddle in the unit interval with the following exponential decay law: $N(n) \sim \exp(-n/\tau)$, where $\tau = \{\ln[\eta/(\eta-1)]\}^{-1}$ is the average lifetime of trajectories on the chaotic saddle [Ott, 1993].

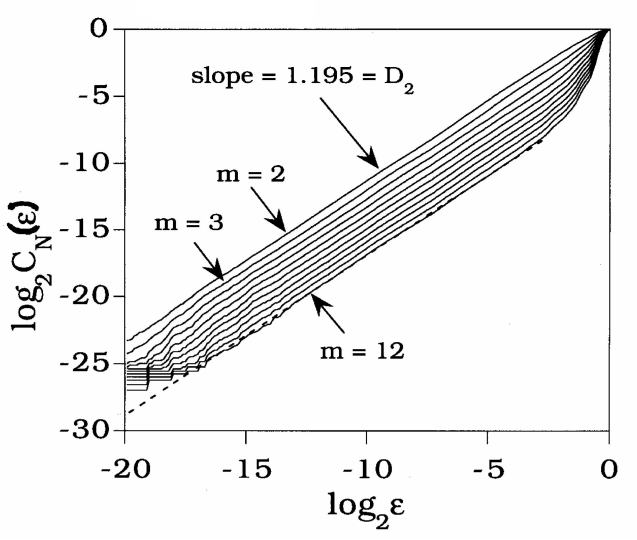

Fig. 9. Plots of the correlation integral on a logarithmic scale for $m = 1, \ldots, 8$. Least-squares fits give $D_2 \approx 1.2$ for $m \geq 2$.

trajectories. The standard approach is to choose an ensemble of initial conditions and ask where the resulting trajectories can be at different times. In particular, since trajectories escape from the chaotic saddle along the unstable manifold, at large positive time n, the $N(n)$ trajectory points will be in the vicinity of the unstable manifold. In order for the points to stay near the unstable manifold at time n, initially these points have to be in the vicinity of the stable manifold. In an intermediate time, the points are then concentrated near the chaotic saddle itself. These considerations lead to the formal definitions of the natural measures of the unstable manifold, the stable manifold, and the chaotic saddle [Grebogi *et al.*, 1988; Hsu *et al.*, 1988; Hunt *et al.*, 1996], as follows.

Let C be a small box within S that contains part of the unstable manifold. The natural measure associated with the unstable manifold in C is

$$\mu_u(C) = \lim_{n\to+\infty} \lim_{N_0\to\infty} \frac{N_u(n, C)}{N(n)}, \qquad (13)$$

where $N_u(n, C)$ is the number of the $N(n)$ orbits in C at time n. Similarly, the natural measure of the stable manifold in a box C in S can be defined as

$$\mu_s(C) = \lim_{n\to+\infty} \lim_{N_0\to\infty} \frac{N_s(n, C)}{N(n)}, \qquad (14)$$

where $N_s(n, C)$ is the *number of initial conditions* in C whose trajectories do not leave S before time n. The definitions (13) and (14) mean that the natural measures associated with the stable and the unstable manifolds in C are determined by the numbers of trajectory points in C at time zero and time n, respectively. The natural measure of the chaotic saddle, μ, can then be obtained by considering $N_m(\rho, n, C)$, the number of trajectory points in C at a time ρn in between zero and n,

$$\mu(C) = \lim_{n\to+\infty} \lim_{N_0\to\infty} \frac{N_m(\rho, n, C)}{N(n)}, \qquad (15)$$

where $0 < \rho < 1$, $N_m(0, n, C) = N_s(n, C)$, and $N_m(1, n, C) = N_u(n, C)$. For large N_0 and n, trajectories that remain in S stay near the chaotic saddle for most of the time between 0 and n, except at the beginning when they are attracted toward the saddle along the stable manifold, and at the end when they are exiting along the unstable manifold. Thus, the measure defined in Eq. (15) is independent of ρ, insofar as $0 < \rho < 1$.

Based on Eq. (15), the following dimension spectrum can be defined for nonattracting chaotic saddles [Tél, 1990], in analogy to that of the chaotic attractor [Grassberger & Procaccia, 1983b; Farmer *et al.*, 1983],

$$D_q = \frac{1}{(q-1)} \lim_{\varepsilon\to 0} \frac{\ln I(q, \varepsilon)}{\ln \varepsilon}, \qquad (16)$$

where q is a continuous index, $I(q, \varepsilon) = \sum_{i=1}^{N(\varepsilon)} \mu_i^q$, μ_i is the natural measure of the chaotic saddle contained in the ith box, and the sum is over all the $N(\varepsilon)$ boxes in a grid of size ε needed to cover the whole chaotic saddle. Setting $q = 2$ gives,

$$D_2 = \lim_{\varepsilon\to 0} \frac{\ln \sum_{i=1}^{N(\varepsilon)} \mu_i^2}{\ln \varepsilon} = \lim_{\varepsilon\to 0} \frac{\ln \langle \mu_i \rangle}{\ln \varepsilon}, \qquad (17)$$

where $\langle \cdot \rangle$ denotes the phase-space average over the chaotic saddle. For an ergodic trajectory on the chaotic saddle, $\langle \mu_i \rangle$ is approximately the probability that the trajectory comes in the ε-neighborhood of a point $\mathbf{x}_i$ on the chaotic saddle in the ith box, which is given by the correlation sum in Eq. (10). From measurements, one does not have a long, ergodic trajectory on the chaotic saddle. Instead, K transient chaotic time series are available, each of length L. The probability p_i that the reconstructed trajectory comes to the neighborhood of $\mathbf{x}_i$ is then

$$p_i \approx \frac{1}{K} \frac{1}{L(L-1)} \sum_{m=1}^{K} \sum_{j=1}^{L} \Theta(\varepsilon - \|\mathbf{x}_j^m - \mathbf{x}_i\|),$$

where $\mathbf{x}_j^m$ is the jth trajectory point reconstructed from the mth transient time series. Since K is in fact the number N_0 of initial conditions in the definition (15), the natural measure μ_i is

$$\mu_i \approx \frac{Kp_i}{Ke^{-L/\tau}} \approx \frac{e^{L/\tau}}{KL(L-1)} \sum_{m=1}^{K} \sum_{j=1}^{L} \Theta(\varepsilon - \|\mathbf{x}_j^m - \mathbf{x}_i\|) \,.$$

Averaging over all points $\mathbf{x}_i$ in the reconstructed phase space gives

$$\langle \mu_i \rangle \approx e^{L/\tau} C_{K,L}(\varepsilon, d) \,, \tag{18}$$

where

$$C_{K,L}(\varepsilon, d) \equiv \frac{1}{KL(L-1)} \sum_{m=1}^{K} \sum_{i=1}^{L} \sum_{j=1, j\neq i}^{L} \Theta(\varepsilon - \|\mathbf{x}_j^m - \mathbf{x}_i^m\|) \tag{19}$$

is the correlation integral associated with K observations of transient chaos, each consisting of L points in the reconstructed phase space. The correlation dimension is then given by

$$D_2 = \lim_{\varepsilon \to 0, K \to \infty} \frac{\ln C_{K,L}(\varepsilon, d)}{\ln \varepsilon} \,. \tag{20}$$

Equation (20) indicates that, if one computes the correlation integral as defined in (19), the GP formulation is valid for transient chaotic time series as well.

To provide numerical support, transient chaotic time series from the Hénon map are used [Dhamala *et al.*, 2001] for which the correlation dimension can be obtained both from the GP formulation Eq. (20) and from a straightforward implementation of the box-counting definition (16) by utilizing a long trajectory on the chaotic saddle [Nusse & Yorke, 1989]. For $a = 1.5$ and $b = 0.3$, there is a chaotic saddle in the phase-space region: $[-2, 2] \times [-2, 2]$ with lifetime $\tau \approx 30$. The box-counting approach gives $D_2 \approx 1.2$. To apply the GP algorithm, $K = 5000$ transient chaotic time series are used [Dhamala *et al.*, 2001]. To guarantee that each time series reflects, approximately, the natural measure of the chaotic saddle, both the initial and the final phases are disregarded, and only 20 points from the middle of the time series are kept. For a given embedding dimension d, the number of trajectory points corresponding to each time series is then $L < 20$. The delay time is chosen to be $T = 1$, each time series is normalized to the unit interval, and the correlation sum $C_{K,L}(\varepsilon, d)$ is computed for 100 values of ε for $-30 < \log_2 \varepsilon < 0$ using embedding dimensions ranging from $d = 1$ to $d = 8$, as shown in Fig. 10(a). For $d > 3$, the local slopes of the plots appear to converge to a plateau value, as shown in Fig. 10(b), which yields $D_2 \approx 1.2$. This agrees well with the value of D_2 obtained from the box-counting algorithm. Note that due to the availability of only short time series, the embedding dimension needs to be much larger than the value of D_2 itself to yield the correct plateau value for D_2, in contrast to the case of long time series from chaotic attractors where $m \approx D_2$ usually suffices [Ding *et al.*, 1993].

2.4. *Computing Lyapunov exponents from time series*

The Lyapunov exponents characterize how a set of orthonormal, infinitesimal distances evolve under the dynamics. For a chaotic system, there is at least one positive Lyapunov exponent — let $\lambda_1 > 0$ be the largest exponent. The defining property of chaos is sensitive dependence on initial conditions, in the following sense. Given an initial infinitesimal distance $\Delta x(0)$, its evolution obeys

$$\Delta x(t) = \Delta x(0) e^{\lambda_1 t} \,.$$

For a M-dimensional dynamical system, there are M Lyapunov exponents. Here we describe a procedure for computing all the exponents from time series [Eckmann *et al.*, 1986].

Consider a dynamical system described by the following equation:

$$\frac{d\mathbf{x}}{dt} = \mathbf{F}(\mathbf{x}) \,, \tag{21}$$

where $\mathbf{x} \in \mathbf{R}^M$ is a M-dimensional vector. Taking variation of both sides of Eq. (21) yields the following equation governing the evolution of the infinitesimal vector $\delta\mathbf{x}$ in the tangent space at $\mathbf{x}(t)$:

$$\frac{d\delta\mathbf{x}}{dt} = \frac{\partial \mathbf{F}}{\partial \mathbf{x}} \cdot \delta\mathbf{x} \,. \tag{22}$$

Solving for Eq. (22) gives

$$\delta\mathbf{x}(t) = \mathbf{A}^t \delta\mathbf{x}(0) \,, \tag{23}$$

where $\mathbf{A}^t$ is a linear operator that evolves an infinitesimal vector at time 0 to time t. The mean

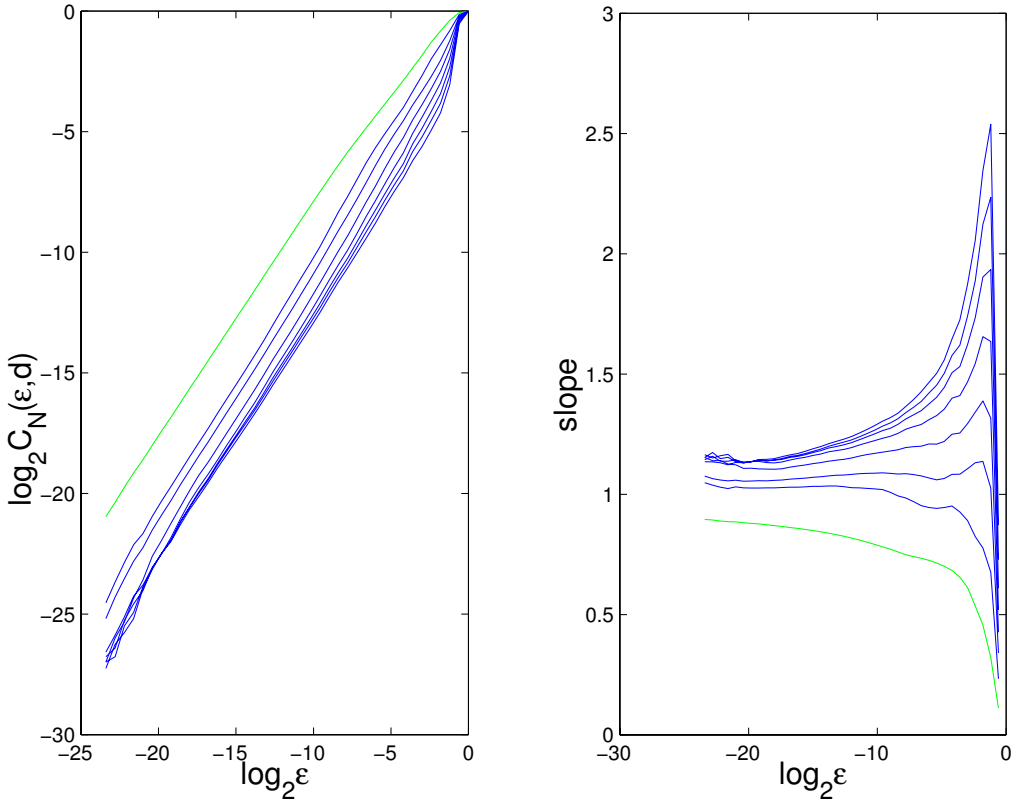

(a) (b)

Fig. 10. For Hénon map, (a) $\log_2 C(\varepsilon, d)$ versus $\log_2 \varepsilon$, and (b) $\log_2 C(\varepsilon, d)/\log_2 \varepsilon$ versus $\log_2 \varepsilon$ at $a = 1.5$, $b = 0.3$. The curves with comparatively higher slopes correspond to higher embedding dimensions.

exponential rate of divergence of the tangent vector is then given by

$$\lambda[\mathbf{x}(0),\, \delta\mathbf{x}(0)] = \lim_{t\to\infty} \frac{1}{t} \ln \frac{\|\delta\mathbf{x}(t)\|}{\|\delta\mathbf{x}(0)\|}\,, \qquad (24)$$

where $\|\cdot\|$ denotes length of the vector inside with respect to a Riemannian metric. In typical situations there exists a d-dimensional basis vector $\{\mathbf{e}_i\}$, in the following sense:

$$\lambda_i \equiv \lambda[\mathbf{x}(0),\, \mathbf{e}_i]\,. \qquad (25)$$

These λ_i's define the Lyapunov spectrum, which can be ordered, as follows:

$$\lambda_1 \geq \lambda_2 \geq \cdots \geq \lambda_d\,. \qquad (26)$$

For chaotic systems, values of λ_i do not depend on the choice of the initial condition $\mathbf{x}(0)$, insofar as $\mathbf{x}_0$ is chosen randomly.

If the system equation (21) is known, then λ_i's can be computed using the standard procedure developed by Benettin *et al.* [1980]. For chaotic time series, there exist several methods for computing the Lyapunov spectrum [Wolf *et al.*, 1985; Sano & Sawada, 1985; Eckmann & Ruelle, 1985; Eckmann *et al.*, 1986; Brown *et al.*, 1991]. While details of these methods are different, they share the same basic principle. Here we describe the one developed by Eckmann *et al.* [1986]. The algorithm consists of three steps: (1) to reconstruct the dynamics using delay-coordinate embedding and search for neighbors for each point in the embedding space, (2) to compute the tangent maps at each point by least-squares fit, and (3) to deduce the Lyapunov exponents from the tangent maps.

2.4.1. *Searching for neighbors in the embedding space*

Given an m-dimensional reconstructed vector time series, in order to determine tangent maps, it is necessary to search for neighbors, i.e. search for $\mathbf{x}_j$ such that:

$$\|\mathbf{x}_j - \mathbf{x}_i\| \leq r\,, \qquad (27)$$

where, r is a small number, and $\|\cdot\|$ is defined as:

$$\|\mathbf{x}_j - \mathbf{x}_i\| = \max_{0\le\alpha\le m-1} |x_{j+\alpha} - x_{i+\alpha}| \,. \tag{28}$$

Such a definition of the distance is only for the consideration of computational speed. If $m = 1$, the time series can be sorted to yield:

$$x_{\Pi(1)} \le x_{\Pi(2)} \le \cdots \le x_{\Pi(N)} \,, \tag{29}$$

where Π is the permutation which, together with its inverse Π^{-1}, are stored. The neighbors of x_i can then be obtained by looking at $k = \Pi^{-1}(i)$ and scanning the sorted time series $x_{\Pi(s)}$ for $s = k \pm 1$, $k \pm 2, \ldots$ until $|x_{\Pi(s)} - x_i| > r$. When $m > 1$, values of s are first selected for which

$$|x_{\Pi(s)} - x_i| \le r \,, \tag{30}$$

as for the case where $m = 1$. The following conditions are further imposed:

$$|x_{\Pi(s)+\alpha} - x_{i+\alpha}| \le r \,, \quad \alpha = 1,\, 2, \ldots,\, m-1 \,, \tag{31}$$

resulting in a complete set of neighbors of $\mathbf{x}_i$ within distance r.

2.4.2. *Computing the tangent maps*

The task is to determine the $m \times m$ matrix T_i which describes how the dynamics send small vectors around $\mathbf{x}_i$ to small vectors around $\mathbf{x}_{i+1}$,

$$T_i(\mathbf{x}_j - \mathbf{x}_i) \approx \mathbf{x}_{j+1} - \mathbf{x}_{i+1} \,. \tag{32}$$

A serious problem is that T_i may not span $\mathbf{R}^m$ because m is usually much larger than the actual phase-space dimension of the system to guarantee a proper embedding. Eckmann *et al.* proposed a strategy that allows T_i to be a $d_M \times d_M$ matrix, where $d_M \le m$. In such a case, T_i corresponds to the time evolution from $\mathbf{x}_i$ to $\mathbf{x}_{i+m}$, and

$$m = (d_M - 1)l + 1 \,, \quad l \ge 1 \,. \tag{33}$$

A new set of embedding vectors can then be constructed:

$$\mathbf{y}_i = (x_i,\, x_{i+l}, \ldots,\, x_{i+(d_M-1)l}) \,. \tag{34}$$

The new vector $\mathbf{y}_i$ is obtained by taking every mth element in the time series and, hence, T_i is defined in the new embedding space, as follows:

$$T_i(\mathbf{y}_j - \mathbf{y}_i) \approx \mathbf{y}_{j+l} - \mathbf{y}_{i+l} \,. \tag{35}$$

Or,

$$T_i \begin{pmatrix} x_j - x_i \\ x_{j+l} - x_{i+l} \\ \cdots \\ x_{j+(d_M-2)l} - x_{i+(d_M-2)l} \\ x_{j+(d_M-1)l} - x_{i+(d_M-1)l} \end{pmatrix} = \begin{pmatrix} x_{j+l} - x_{i+l} \\ x_{j+2l} - x_{i+2l} \\ \cdots \\ x_{j+(d_M-1)l} - x_{i+(d_M-1)l} \\ x_{j+d_M l} - x_{i+d_M l} \end{pmatrix} \tag{36}$$

Therefore, T_i can be expressed as:

$$T_i = \begin{pmatrix} 0 & 1 & 0 & \cdots & 0 \\ 0 & 0 & 1 & \cdots & 0 \\ \cdots & \cdots & \cdots & \cdots & \cdots \\ 0 & 0 & 0 & \cdots & 0 \\ a_1 & a_2 & a_3 & \cdots & a_{d_M} \end{pmatrix} \tag{37}$$

The task of finding T_i then reduces to that of finding the set of d_M matrix elements a_i ($i = 1,\, 2, \ldots,\, d_M$). This can be accomplished by using a least-squares fit. Let $S_i^E(r)$ be the set of indices j of neighbors $\mathbf{x}_j$ of $\mathbf{x}_i$ within distance r. The procedure is to minimize the quantity

$$\sum_{j\in S_i^E(r)} \left[\sum_{k=0}^{d_M-1} a_{k+1}(x_{j+kl} - x_{i+kl}) - (x_{j+d_M l} - x_{i+d_M l}) \right]^2 . \tag{38}$$

A critical quantity is $S_i^E(r)$. If $S_i^E(r)$ is large, the computation required is intensive. On the other hand, if $S_i^E(r)$ is too small, the least-squares fit may fail. Generally, it is necessary to choose r sufficiently large so that $S_i^E(r)$ contains at least d_M elements. But r also needs to be small so that the linear dynamics approximation about every $\mathbf{x}_i$ is valid. Eckmann *et al.* suggest the following empirical rule for choosing r: Count the number of neighbors of $\mathbf{x}_i$ corresponding to increasing values of r from a preselected sequence of possible values, and stop when the number of neighbors exceeds $\min(2d_M,\, d_{M+4})$ for the first time. Increase r further if T_i is singular.

2.4.3. *Computing the exponents*

To compute the Lyapunov exponents from the tangent maps is relatively straightforward. Eckmann and Ruelle [1985] suggest the following procedure. Starting from an identity matrix $Q_{(0)} \equiv I$, the following matrix decomposition (QR-decomposition) can be done:

$$\begin{aligned} T_1 Q_{(0)} &= Q_{(1)} R_{(1)} \,, \\ T_{1+m} Q_{(1)} &= Q_{(2)} R_{(2)} \,, \\ &\vdots \,, \\ T_{1+jm} Q_{(j)} &= Q_{(j+1)} R_{(j+1)} \,, \\ &\vdots \,, \end{aligned} \tag{39}$$

where $Q_{(j)}$'s are orthogonal matrices, and $R_{(j)}$'s are upper triangular matrices with positive diagonal elements. The above decomposition is robust, an algorithm of which can be found in [Press *et al.*, 1986]. The Lyapunov exponents are then given by

$$\lambda_k = \frac{1}{l\tau k} \sum_{j=0}^{K-1} \ln R_{(j)kk} \,, \tag{40}$$

where $R_{(j)kk}$ is the kth diagonal elements of the matrix $R_{(j)}$, and $K \leq (N - d_M l - 1)/l$ is the number of available matrices.

2.4.4. *Remarks*

The algorithm described above is robust. In particular, it can compute all the positive Lyapunov exponents reliably [Eckmann *et al.*, 1986], although the correct identification of the negative exponents remains a challenging issue [Sauer *et al.*, 1998; Sauer & Yorke, 1999]. Three points need to be stressed. Firstly, d_M cannot be too large, otherwise spurious exponents may arise. Generally, d_M should be larger than the number of positive exponents. Secondly, the choice of r is critical, as discussed above. In the presence of noise, it may be good to replace the ball $\{\mathbf{x}_j : \|\mathbf{x}_j - \mathbf{x}_i\| \leq r\}$ by a shell $\{\mathbf{x}_j : r_{\min} < \|\mathbf{x}_j - \mathbf{x}_i\| \leq r\}$ when searching for neighbors. Thirdly, increasing the number of points in the time series at fixed recording time is useless. In order to improve the computation, the total recording time should be increased.

In brief summary, when computing the Lyapunov exponents from time series, the following rules should be followed:

1. Use long recording time, but not very small sampling time step τ;
2. Use large embedding dimension m;
3. Use a matrix dimension d_M somewhat larger than the expected number of positive Lyapunov exponents;
4. Choose r such that the number of neighbors is greater than the smaller of $2d_M$ and d_{M+4};
5. Otherwise keep r as small as possible;
6. Take a product of as many matrices as possible to determine the Lyapunov exponents.

2.4.5. *A numerical example*

Here we discuss the computation of the Lyapunov exponents from an ensemble of transient chaotic time series using the procedure described above. Again, consider the Hénon map in a parameter region where the map generates transient chaos. In [Dhamala *et al.*, 2001], an ensemble of chaotic transients is generated from the Hénon map for the parameter pairs $(a, b) = (1.46, 0.3)$ and $(a, b) = (1.50, 0.3)$, and 21,000 points near each chaotic saddle are accumulated by using 300 random initial conditions in $[-2, 2] \times [-2, 2]$ for the case $a = 1.46$ and 700 random initial conditions for $a = 1.50$. (The average lifetime of the chaotic transients is about 70 iterates for $a = 1.46$ and 30 iterates for $a = 1.50$.) A two-dimensional embedding with a time delay of 1 is constructed from each collection of time series. Local linear maps are computed using least squares for each neighborhood.

In the case $a = 1.46$, each transient time series consists of about 70 iterates. Thus, the Lyapunov exponents computed are actually finite-time approximations, where a suitable product of the 70 or so linear maps associated with points on the individual transient time series is considered. Similarly, when $a = 1.50$, it is necessary to consider products of 30 or so linear maps. Figure 11(a) shows the distribution of the largest Lyapunov exponent, λ_1, computed from the ensembles of time series for $a = 1.46$, and Fig. 11(b) shows the distribution of the values of λ_2. It can be seen that $\lambda_1 = 0.44 \pm 0.05$ and $\lambda_2 = -1.72 \pm 0.06$. Similarly, for $a = 1.50$, the exponents are: $\lambda_1 = 0.54 \pm 0.06$ and $\lambda_2 = -1.77 \pm 0.08$. The estimated values of the exponents agree reasonably well with the theoretical ones [Dhamala *et al.*, 2001].

3. Time-Frequency Analysis of Chaotic Time Series

The method of chaotic time series analysis described in Sec. 2 is applicable to low-dimensional,

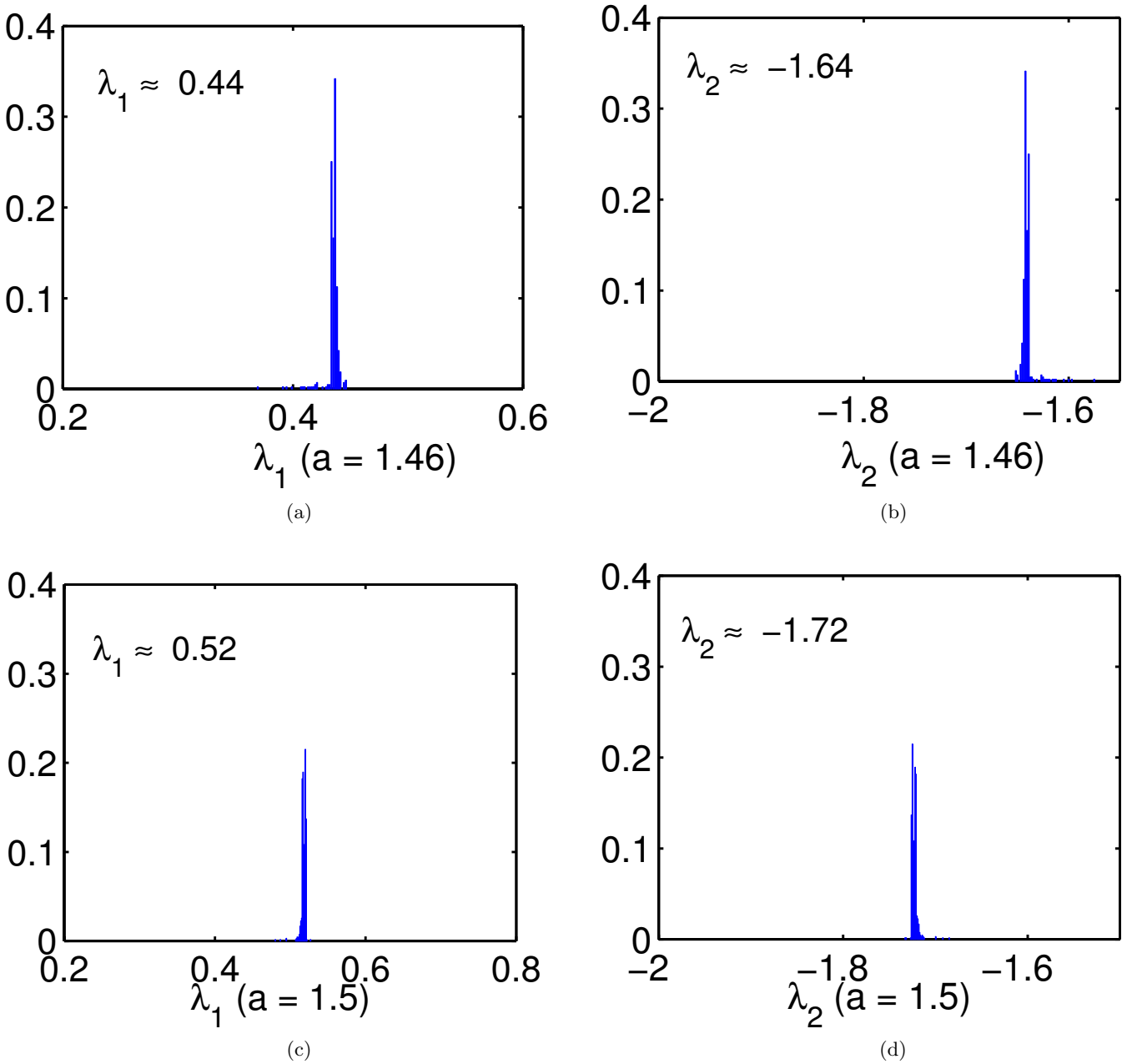

Fig. 11. (a–d) The distributions of Lyapunov exponents of the Hénon map for chaotic transients at the two parameter values of $a = 1.46$ and 1.50, respectively.

low-noise deterministic dynamical systems. For more general and more complicated signals, time-frequency analyses are still commonly used. An excellent discussion and comparison of various time-frequency methods can be found in [Huang *et al.*, 1998]. These are: (1) the traditional Fourier method, (2) the wavelet method, and (3) the Hilbert transform method. In what follows we briefly discuss the Fourier and wavelet methods, following mainly the discussion in [Huang *et al.*, 1998]. We will then focus on the Hilbert transform and give examples to illustrate its usefulness for chaotic signal processing.

Fourier spectral analysis is traditionally the time series analysis method, which can be found in many standard textbooks. A necessary condition for the Fourier analysis to be meaningful is that the time series should be piecewise stationary. Even then, there are common situations where the Fourier analysis cannot yield much

information, such as deterministic chaotic time series with broad-band power spectra for which the Fourier spectrum gives absolutely no indication about the deterministic origin, let alone the fundamental invariants of the underlying dynamical system. There exist other technical difficulties associated with the Fourier analysis. For instance, when a set of windows is chosen from a piecewise stationary time series for Fourier analysis, how can one guarantee that the window width coincides with the stationary time scale? In order to detect events localized in time, the window width must be small, which usually results in poor resolution in the frequency domain. Therefore, in general, the Fourier method is useful for stationary time series. It is particularly powerful if the underlying system generating the time series is linear.

In recent years, the wavelet analysis has become more popular for the analysis of nonstationary time series, which is essentially an *adjustable* window Fourier spectral analysis. In general, for a time series $x(t)$, the wavelet transform is

$$W(a,\, b) = \frac{1}{\sqrt{|a|}} \int_{-\infty}^{\infty} x(t)\psi^* \left(\frac{t-b}{a}\right) dt\,, \qquad (41)$$

where $\psi^*(\cdot)$ is the basic wavelet function that satisfies certain general conditions, a is the dilation factor and b is the translation parameter. While time and frequency do not appear explicitly in $W(a,\, b)$, the variable $1/a$ gives the frequency scale and b indicates the temporal location of an event. Physically, $W(a,\, b)$ is the energy of $x(t)$ in scale a about $t = b$. For different problems, the choices of the wavelet function $\psi^*(\cdot)$ are usually different. For instance, a commonly used function is the Morlet wavelet, which is essentially Gaussian enveloped sine and cosine waves [Chan, 1995]. The wavelet analysis is fundamentally a linear method. While it provides a uniform energy resolution for all the scales, the resolution is generally poor because the size of the basic wavelet function is limited [Huang *et al.*, 1998]. In the past decade or so, there has been a tremendous amount of work on wavelet analysis, particularly in the applied mathematics literature. Successful applications include edge detection and image compression [Chan, 1995].

Recently, a method based on the Hilbert transform has been proposed, which can be suitable for nonstationary, nonlinear and/or random time series. The method, pioneered by Huang *et al.* [1998], has been demonstrated to be useful for a number of applications.

3.1. *Analytic signals and the Hilbert transform*

3.1.1. *Analytic signals*

Signals in the physical world are real. Nevertheless, in a variety of applications such as optics, it is convenient to represent real signals by complex ones. The concept of *analytic signals*, first proposed by Gabor [1946] in his study of optical holograph, is a natural way to define a complex signal with a clear physical meaning. In particular, given a real signal $x(t)$, one performs a mathematical transform to obtain the corresponding imaginary part $\tilde{x}(t)$, yielding a complex signal $\psi(t)$:

$$\psi(t) = x(t) + i\tilde{x}(t) = A(t)e^{i\phi(t)}\,.$$

Suppose that the imaginary part can be obtained uniquely through the mathematical transform in the sense that the analytic signal $\psi(t)$ corresponds geometrically to a rotation, its amplitude and phase can then be defined, as follows:

$$A(t) = \sqrt{x(t)^2 + \tilde{x}(t)^2}\,, \quad \phi(t) = \arctan\left[\frac{\tilde{x}(t)}{x(t)}\right].$$

The phase variable $\phi(t)$ gives the *instantaneous frequency* $\omega(t)$:

$$\omega(t) = \frac{d\phi(t)}{dt} = \frac{x(t)\dot{\tilde{x}}(t) - \dot{x}(t)\tilde{x}(t)}{A^2(t)}\,. \qquad (42)$$

Note that the instantaneous frequency $\omega(t)$ is fundamentally different from the concept of frequency in the Fourier transform defined in the base of simple harmonic functions. Here, the base is the physically meaningful concept of rotations. The instantaneous frequency $\omega(t)$ measures the rate of rotation in the complex plane of the corresponding analytic signal.

The main issue is then how to define the imaginary part of complex signal. Interest in the proper definition of the imaginary part first arose with the advent of frequency modulation for radio transmission in the 1920s. The necessity for the notion of instantaneous frequency, which quantifies the rate of change of phase angle, was clearly identified and a general scheme was proposed, but a good definition of phase angle was missing at the time. It was Gabor [1946] who proposed a solution to the problem by inventing the analytic signal.

Gabor's approach is as follows. Observe that if the real signal $x(t)$ has a Fourier transform $S(\omega)$,

then the complex signal, $\psi(t)$, whose spectrum is composed of positive frequencies of $S(\omega)$ only, is given by the inverse transform of $S(\omega)$, where the integration goes only over the positive frequencies:

$$\psi(t) = \frac{2}{\sqrt{2\pi}} \int_0^\infty S(\omega) e^{i\omega t} d\omega$$

The factor 2 is inserted so that the real part of the analytical signal is $x(t)$, not one half of that. The explicit form of $\psi(t)$ can then be obtained in terms of the real signal $x(t)$. Since

$$S(\omega) = \frac{1}{\sqrt{2\pi}} \int_{-\infty}^\infty x(t) e^{-i\omega t} dt\,,$$

the complex signal can be written as

$$\begin{aligned}\psi(t) &= 2\frac{1}{2\pi} \int_0^\infty \int_{-\infty}^\infty x(t') e^{-i\omega t'} e^{i\omega t} dt' d\omega \\ &= \frac{1}{\pi} \int_0^\infty \int_{-\infty}^\infty x(t') e^{-i\omega(t-t')} dt' d\omega\,. \end{aligned} \quad (43)$$

The mathematical identity [Arfken & Weber, 1995]

$$\int_0^\infty e^{i\omega\tau} d\omega = \pi\delta(\tau) + \frac{i}{\tau}$$

gives

$$\psi(t) = \frac{1}{\pi} \int_{-\infty}^\infty x(t') \left[\pi\delta(t-t') + \frac{i}{t-t'}\right] dt'\,,$$

which yields [Hahn, 1996]

$$\psi(t) = x(t) + i\frac{1}{\pi} \int_{-\infty}^\infty \frac{x(t')}{t-t'} dt'\,, \quad (44)$$

the analytic signal corresponding to the real signal $x(t)$. The imaginary part of Eq. (44) is nothing but the Hilbert transform $\tilde{x}(t)$ of the real signal $x(t)$,

$$\tilde{x}(t) = P.V. \left[\frac{1}{\pi} \int_{-\infty}^\infty \frac{x(t')}{t-t'} dt'\right]\,, \quad (45)$$

where *P.V.* stands for the Cauchy principal value for the integral. In principle, there are many ways to define a complex function from $x(t)$, but the Hilbert transform provides a unique way to define $\tilde{x}(t)$ (also known as the *quadrature signal* [Okunev, 1997]) so that $\psi(t)$ has an analytic continuation over the complex upper half-plane. From a physical standpoint, $x(t)$ represents some physical measurement and also serves as a boundary condition for defining some analytic function.

3.1.2. *The Hilbert transform*

To better understand the meaning of the Hilbert transform, we examine some mathematical issues. Consider the following one-dimensional integral-transform pair:

$$u(t) \Leftrightarrow U(s)$$

where a time function $u(t)$ is transformed into a complex function of a real variable s. This notation may also be written in the form of the following pair of integrals [Hahn, 1996]:

$$U(s) = \frac{1}{\pi} \int_{-\infty}^\infty \frac{u(t)}{s-t} dt$$

$$u(t) = \frac{1}{\pi} \int_{-\infty}^\infty \frac{U(s)}{t-s} ds\,.$$

A look at these integrals reveals that the Hilbert transforms are defined using the kernel $1/\pi(s-t)$ and the conjugate kernel $1/\pi(t-s)$. In general, the Hilbert transforms are written in a more explicit form:

$$\tilde{u}(t) = P.V. \left[\frac{-1}{\pi} \int_{-\infty}^\infty \frac{u(\tau)}{\tau-t} d\tau\right]\,, \quad (46)$$

$$u(t) = P.V. \left[\frac{1}{\pi} \int_{-\infty}^\infty \frac{\tilde{u}(\tau)}{\tau-t} d\tau\right]\,. \quad (47)$$

The integrals in these equations are improper integrals in the sense of the Cauchy principal value. For Eq. (47), the integral is defined by the limit [Hahn, 1996]:

$$u(t) = \lim_{\varepsilon\to 0;\, L\to\infty} \frac{1}{\pi} \left\{\int_{-L}^{t-\varepsilon} \frac{\tilde{u}(\tau)}{\tau-t} d\tau + \int_{t+\varepsilon}^{L} \frac{\tilde{u}(\tau)}{\tau-t} d\tau\right\}.$$

Essentially, Eqs. (46) and (47) define convolution, which can be seen by applying the change of variable ($\tau \to t-\tau$) to the Hilbert transform given in Eq. (46). This yields

$$\tilde{u}(t) = \int_{-\infty}^\infty \frac{u(t-\tau)}{\pi\tau} d\tau\,, \quad (48)$$

where the integral again is to be taken as the Cauchy principal value. This form of Hilbert transform clearly shows that $\tilde{u}(t)$ is the convolution of $u(t)$ with $1/\pi t$, i.e.

$$\begin{aligned}\tilde{u}(t) &= \frac{1}{\pi t} * u(t)\,, \\ u(t) &= \frac{-1}{\pi t} * \tilde{u}(t)\,, \end{aligned} \quad (49)$$

where $*$ denotes the convolution operation.

3.1.3. *Numerical computation of the analytical signal*

The key to numerically computing the analytic signal is the relation between the Hilbert and the Fourier transforms. In particular, the Hilbert transform of $x(t)$ is the positive part of the Fourier transform of $x(t)$, multiplied by two [Frenking, 1994]. This can be seen by examining the convolution given in Eq. (49). Recall that the convolution $g * h$ is one member of a simple transformation pair:

$$g * h \Leftrightarrow \mathcal{FT}(g)\mathcal{FT}(h)\,,$$

where $\mathcal{FT}$ denotes the Fourier transformation, which is the the convolution theorem. We thus have [Shenoi, 1995]

$$\begin{aligned}\frac{1}{\pi t} * u(t) &\Leftrightarrow \mathcal{FT}\left(\frac{1}{\pi t}\right)\mathcal{FT}(u(t)) \\ &\Leftrightarrow -i\,\mathrm{sgn}(\omega)U(\omega)\,, \end{aligned} \tag{50}$$

where $U(\omega)$ is the complex Fourier transform of $u(t)$ and the signum function is [Hahn, 1996] defined as

$$\mathrm{sgn}(\omega) = \begin{cases} +1 & \text{for } \omega > 0 \\ 0 & \text{for } \omega = 0 \\ -1 & \text{for } \omega < 0 \end{cases}.$$

Since $u(t)$ is a real function of time, we have $U(-\omega) = U^*(\omega)$. Then, the analytical signal can be written as

$$\psi(t) = u(t) + i\tilde{u}(t) = 2\frac{1}{\sqrt{2\pi}}\int_0^\infty U(\omega)e^{i\omega t}d\omega\,. \tag{51}$$

This simple result is important because it says that, if the signal can be expressed in the Fourier frequency domain, then the analytic signal can be obtained by dropping negative-frequency terms, multiplying the positive-frequency terms by two, and transforming back to time domain.

3.1.4. *Instantaneous frequency*

Instantaneous frequency, together with phase, is an intuitive concept. The exact mathematical description of the frequency modulation is quite intriguing, but the following simple argument suggests the physical meaning of the definition of the instantaneous frequency as the derivative of the phase variable.

Assume $\psi(t)$ has the spectrum $S(\omega)$, then the mean frequency is given by [Boashash *et al.*, 1995]

$$\begin{aligned}\langle\omega\rangle &= \int \omega|S(\omega)|^2 d\omega \\ &= \frac{1}{2\pi}\iiint \omega\psi^*(t)\psi(t')e^{i\omega(t-t')}d\omega dt' dt \\ &= \frac{1}{2\pi i}\iiint \psi^*(t)\psi(t')\left(\frac{\partial}{\partial t}e^{i\omega(t-t')}\right)d\omega dt' dt \\ &= \frac{1}{i}\iint \psi^*(t)\left(\frac{\partial}{\partial t}\delta(t-t')\right)\psi(t')d\omega dt' dt \\ &= \int \psi^*(t)\frac{1}{i}\left(\frac{d}{dt}\psi(t)\right)dt\,,\end{aligned}$$

which can also be written as

$$\langle\omega\rangle = \int\left[\frac{d}{dt}\phi(t) - \frac{i}{A(t)}\left(\frac{d}{dt}A(t)\right)\right]A^2(t)dt\,.$$

The second term is zero since that term is purely imaginary; it must be zero for $\langle\omega\rangle$ to be real, which gives [Huang *et al.*, 1998]

$$\begin{aligned}\langle\omega\rangle &= \int\left(\frac{d}{dt}\phi(t)\right)|S(\omega)|^2 d\omega \\ &= \int\left(\frac{d}{dt}\phi(t)\right)A^2(t)dt\,.\end{aligned}$$

This is an interesting and important result because it says that the average frequency may be obtained by integrating the instantaneous frequency with the density over all time:

$$\omega(t) = \frac{d}{dt}\phi(t)\,. \tag{52}$$

As an example, Fig. 12(a) shows the plot of $x(t)$ of a simple harmonic oscillator, versus $\tilde{x}(t)$, the Hilbert transform of $x(t)$. For $x(t) = A\,\sin(\omega t)$, where ω is a constant, the Hilbert transform is trivial and can be performed by shifting all frequency components of $x(t)$ by $\pi/2$, i.e. $\tilde{x}(t) = -A\,\cos(\omega t)$. The unwrapped phase function corresponding to Fig. 12(a) is a monotonically increasing straight line as shown in Fig. 12(b), and the instantaneous frequency shown in Fig. 12(c) is constant, as expected.

With these notations, the bandwidth associated with the spectrum of the instantaneous frequency

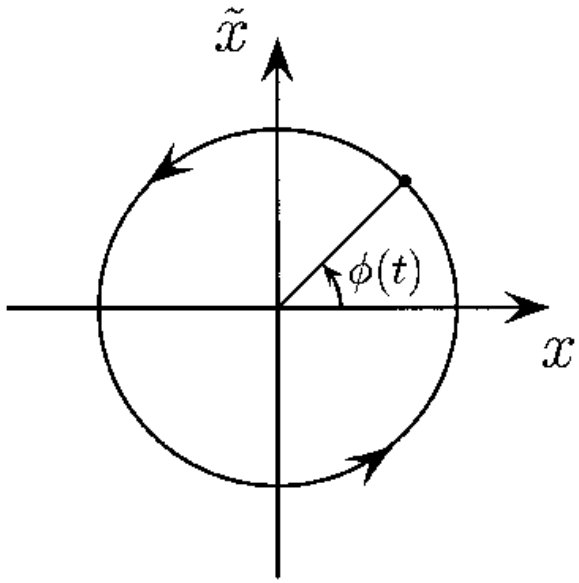

(a)

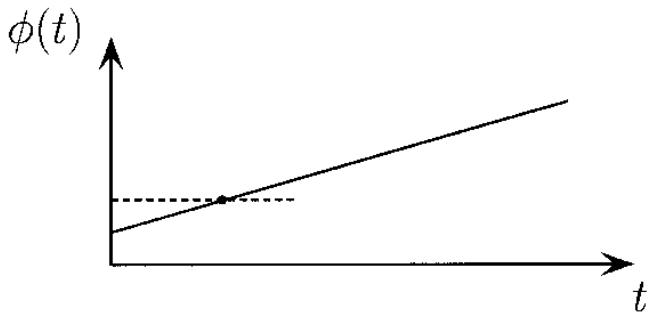

(b)

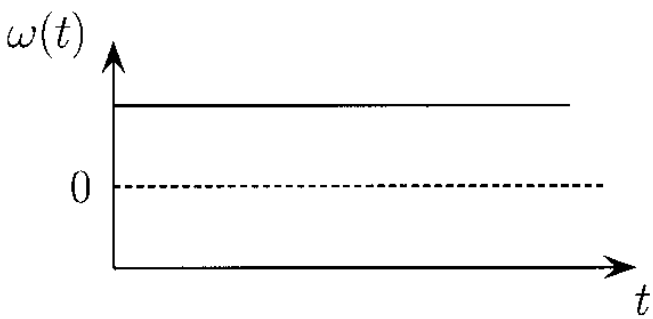

(c)

Fig. 12. Illustration of the Hilbert transform and instantaneous frequency associated with a simple harmonic oscillator: (a) the real signal $x(t)$, (b) its Hilbert transform, and (3) the constant frequency.

can be defined as [Huang *et al.*, 1998]

$$B^2 = \sigma_\omega^2 = \int (\omega - \langle\omega\rangle)^2 |S(\omega)|^2 d\omega$$

$$= \int \psi^*(t) \left(\frac{1}{i}\frac{d}{dt} - \langle\omega\rangle\right)^2 \psi(t) dt$$

$$= \int \left| \left(\frac{1}{i}\frac{d}{dt} - \langle\omega\rangle\right) \psi(t) \right|^2 dt$$

$$= \int \left| \frac{-i}{A(t)} \left(\frac{d}{dt}A(t)\right) + \frac{d}{dt}\phi(t) - \langle\omega\rangle \right|^2 A^2(t) dt\,,$$

or

$$B^2 = \int \left(\frac{d}{dt}A(t)\right)^2 dt + \int \left[\frac{d}{dt}\phi(t) - \langle\omega\rangle\right]^2 A^2(t) dt\,.$$

For a *narrow band signal*, B^2 must be a small, i.e. both the amplitude $A(t)$ and the phase $\phi(t)$ are slowly varying functions of time.

Even with the definition given in Eq. (52) as the derivative of phase, there still is a considerable controversy over the meaning of instantaneous frequency, especially if the signal is not *monocomponent*, a term which was introduced to ensure $\omega(t)$ has a *narrow band spectrum*. Suppose $\phi(t)$ generated by Eq. (44) can be represented by

$$\phi_i(t) = \int_0^t \omega_i(\tau) d\tau\,.$$

Here, i indicates the different components having different oscillatory frequencies. Assume the original signal $x(t)$ can be expressed as [Boashash, 1992]

$$x(t) = \sum_{i=1}^{N} C_i(t) + \eta(t)\,, \tag{53}$$

where $\eta(t)$ represents a residue term with negligible amplitude and N is some finite number. By construction, each C_i is an *intrinsic mode* of $x(t)$ with a simple oscillatory waveform described by the envelopes $A_i(t)$ and the instantaneous frequencies $\omega_i(t)$ such that the analytic signal $\psi_i(t)$ associated with $C_i(t)$ is

$$\psi_i(t) = A_i(t) e^{\phi_i(t)} \quad \text{i.e. } C_i(t) = A_i(t)\cos(\phi_i(t))$$

If $i = 1$, the signal is said to be a mono-component signal; if, however, $i \geq 2$, then the signal is referred to as a multicomponent signal [Boashash, 1992].

Figure 13(a) shows an example of a multicomponent signal. The real part of the signal is $x(t) = A_1 \sin(\omega_1 t) + A_2 \sin(\omega_2 t)$ with $\omega_1 = 1$, $\omega_2 = 3$ and $A_1 = 1$, $A_2 = 0.9$. The spectrum of this signal

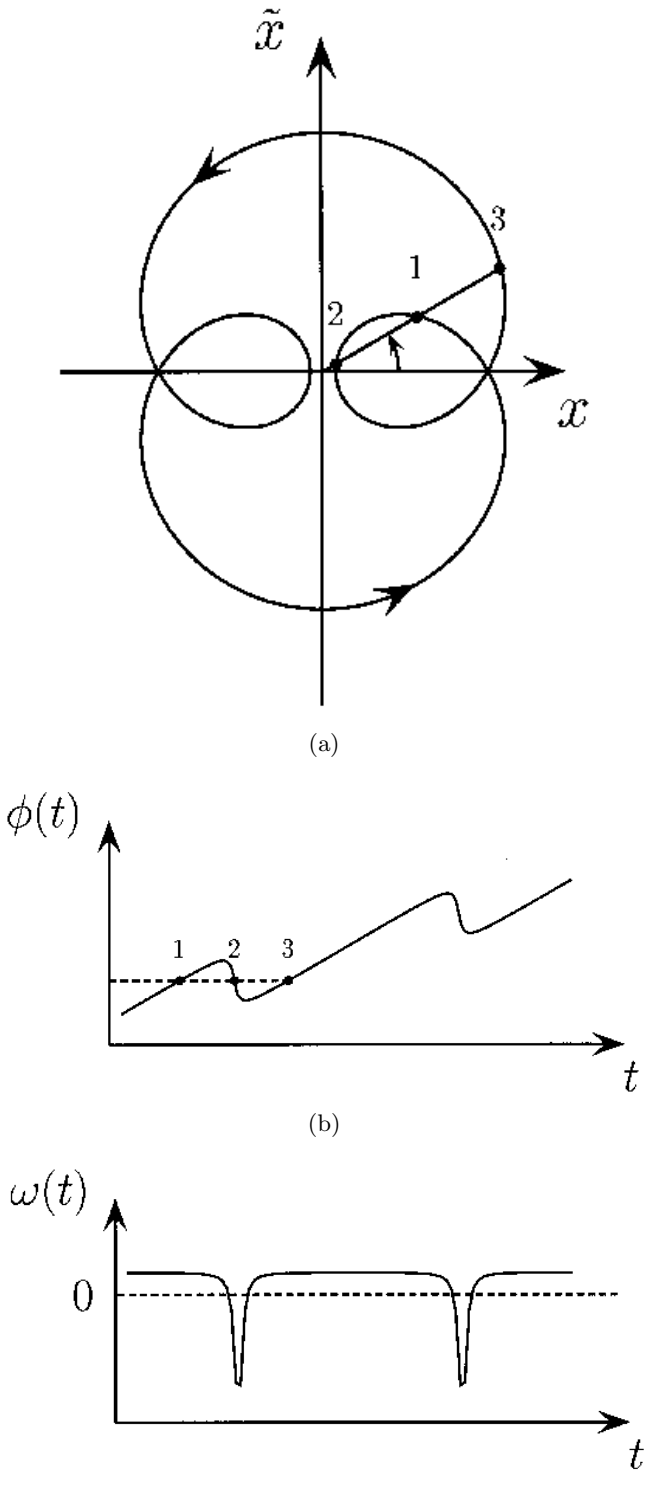

Fig. 13. (a) The plot of $x(t) = \sin(t) + 0.9\sin(3t)$ in its complex plane of analytic signal. The Hilbert transform of the signal is $\tilde{x}(t) = -\cos(t) - 0.9\cos(3t)$. Clearly the rotation is **not** a proper one. The trajectory needs to change the direction of rotation with respect to the origin to pass through the points denoted by 1, 2 and 3. (b) Unwrapped phase function $\phi(t)$ obtained from (a). (c) Time derivative of the phase function in (a) has intervals with negative frequencies which are *unphysical*.

consists of two delta functions at ω_1 and ω_2:

$$S(\omega) = A_1\delta(\omega - \omega_1) + A_2\delta(\omega - \omega_2)\,.$$

Since ω_1 and ω_2 are taken to be positive, the signal is analytic. Solving for the phase and amplitude:

$$\phi(t) = \arctan\frac{A_1\sin(\omega_1 t) + A_2\sin(\omega_2 t)}{A_1\cos(\omega_1 t) + A_2\cos(\omega_2 t)}\,,$$

$$A^2(t) = A_1^2 + A_2^2 + 2A_1A_2\cos(\omega_2 - \omega_1)t$$

and taking the derivative of the phase yield the instantaneous frequency:

$$\omega(t) = \frac{d}{dt}\phi(t) = \frac{1}{2}(\omega_2 + \omega_1) + \frac{1}{2}(\omega_2 - \omega_1)\frac{A_1^2 - A_2^2}{A^2(t)}\,.$$

Notice that due to the last term in the above equation, the trajectory in Fig. 13(a) traces out a rotation with two separate centers. This is also apparent in Fig. 13(b), where the unwrapped phase function is no longer a monotonically increasing function of time. The result of this behavior is evident in the instantaneous frequency plot shown in Fig. 13(c). Clearly, the negative values assumed by the instantaneous frequency are *unphysical*. This example illustrates that even for a simple signal, a meaningful instantaneous frequency can only be obtained if some restrictive conditions are imposed on the data. However, almost all of the conditions discussed in several references [Gabor, 1946; Boashash, 1992; Bedrosian, 1963] are global and do not provide a scheme as to how to obtain the decomposition given in Eq. (53). Recently, Huang *et al.* [1998] introduced the Empirical Mode Decomposition (EMD) method for generating intrinsic modes that are mono-components.

3.2. *Method of empirical mode decomposition*

In order to define physically meaningful instantaneous frequencies, it is necessary that the analytic signal possess a proper structure of rotation. For instance, there should be a unique center of rotation. More precisely, the analytic signal $\psi(t)$ should satisfy the following two conditions in its own complex plane: (1) there is a preferred direction of rotation (e.g. either clockwise or counterclockwise), and (2) the rotation can be defined with respect to a unique center.

The first condition is self-explanatory, and the second condition is a one ensuring that the instantaneous frequency does not have any undesirable fluctuations induced by asymmetric waveforms [Huang *et al.*, 1998]. Physically, these two requirements amount to having a well-behaved rotation-like motion as shown in Fig. 12(a). It is natural to call a rotation satisfying these two conditions in the complex plane of analytic signal a **proper rotation**. For a complicated signal that does not satisfy the above conditions, it is necessary to express it by a sum of proper rotations (if possible). The empirical mode decomposition (EMD) method developed by Huang *et al.* [1998] is such a method. The heart of the decomposition method is to identify the innate undulations belonging to different time scales and sift them out to obtain one intrinsic mode at a time. This can be achieved by making use of the envelopes defined by the local maxima and minima to discern waves riding on top of the others. Once the extrema of the data set are identified, all the local maxima and local minima are connected by a cubic spline to form an upper envelope $s_{\max}(t)$ and a lower envelope $s_{\min}(t)$. Their mean is denoted by

$$m(t) = \frac{s_{\max}(t) + s_{\min}(t)}{2} \tag{54}$$

and it is subtracted (*sifted out*) from the original data $x(t)$ to yield $r(t)$

$$r(t) = x(t) - m(t)\,.$$

Ideally, $r(t)$ should be an intrinsic mode. However, due to the imperfections in the construction of the envelopes, overshoots and undershoots can generate new extrema or modify the existing ones. Therefore $r(t)$ must be checked to see if it satisfies the two conditions specifying a proper rotation. If the conditions are not satisfied, the sifting procedure is carried out again by forming $s_{\max}(t)$ and $s_{\min}(t)$ but this time from $r(t)$. The mean $m(t)$ is calculated by Eq. (54). That is, in the second sifting, $r(t)$ is regarded as the data to be analyzed:

$$r(t) \to r(t) - m(t)\,.$$

By sifting out the local mean $m(t)$ from $r(t)$, some riding waves can be eliminated, yielding wave profiles that are more symmetric. This process of sifting continues until $r(t)$ corresponds to a proper rotation. Then, it is designated as

$$C_1(t) = r(t)\,,$$

which is the first intrinsic mode. In general, $C_1(t)$ contains the highest-frequency oscillations of the original signal since the envelopes are formed using maxima of the fastest riding waves. This shortest time-scale component can be subtracted from the data:

$$x(t) \to x(t) - C_1(t)\,.$$

The remainder can be treated as the new data subjected to the same sifting process described above. This procedure can be applied repeatedly to yield subsequent intrinsic modes $C_i(t)$ belonging to different time scales. The sifting process is stopped when $r(t)$ shows no apparent variations (i.e. it has fewer than two local extrema) or the amplitude of the oscillations in the time domain becomes negligibly small compared with the amplitude of the original signal $x(t)$. The last component is denoted by $\varepsilon(t)$ which is roughly a quadratic or a linear function of time with relatively small amplitude. Summarizing these steps, it can be seen that the original signal $x(t)$ is decomposed in the following manner:

$$x(t) = \sum_{i=1}^{M} C_i(t) + \varepsilon(t)\,,$$

as given in Eq. (53).

3.3. *Application to chaotic systems (I): The Lorenz chaotic signals*

To illustrate the decomposition procedure, we use the data collected from the chaotic attractor of the Lorenz system [Lorenz, 1963]:

$$\begin{aligned} \frac{dx}{dt} &= 16(x - y)\,, \\ \frac{dy}{dt} &= -xz + 45.92x - y\,, \\ \frac{dz}{dt} &= xy - 4z\,. \end{aligned} \tag{55}$$

Figure 14(a) shows the time series obtained from $y(t)$ for $\sigma = 16$, $\rho = 45.92$ and $\beta = 4$. The data appear to be quite complicated. Despite many local extrema, there are relatively fewer zero crossings. The corresponding trajectory in the complex plane of $\psi(t)$ is shown in Fig. 14(b), where it is apparent that the rotation is not proper as it has two centers and, hence, in this case, no proper phase function $\phi(t)$ can be defined. Figure 14(c) shows the trajectory in the complex plane of the first intrinsic mode $C_1(t)$ from the Lorenz system. Now there is a unique

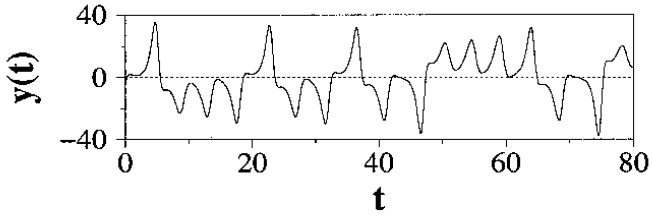

(a)

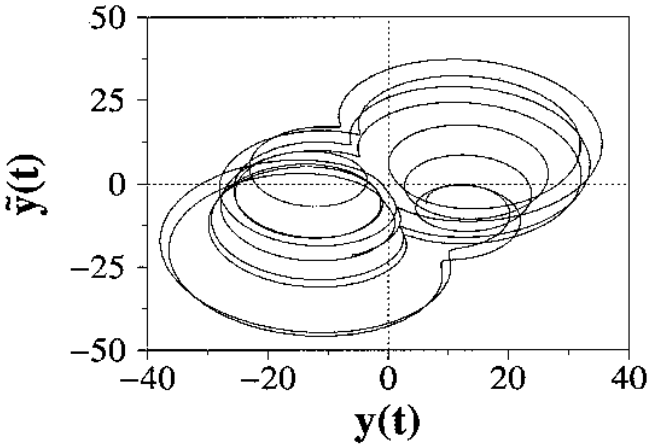

(b)

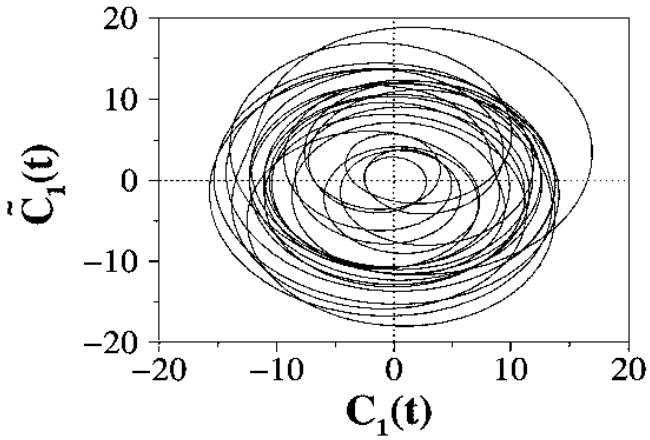

(c)

Fig. 14. (a) A trajectory from y-component of the Lorenz equation. (b) The same trajectory in the complex plane of the analytic signal. The motion exhibits multiple centers of rotation so that a proper phase cannot be defined. (c) A similar trajectory from the first intrinsic mode $C_1(t)$ of $y(t)$ of the Lorenz system. In this case, the phase $\phi_1(t)$ can be properly defined.

center for which the phase of $C_1(t)$ can be defined properly.

The first component $C_1(t)$ shown in Fig. 14(c) is obtained as follows: we first identify the local extrema and obtain upper and lower envelopes. In practice, serious problems can occur near the end points of the original signal $x(t)$ during the spline fitting process. If the edges of the data are left untreated, the spline fittings will introduce large perturbations into the data which can propagate and eventually corrupt the signal. An example of the edge effects is shown in Fig. 15(a). Here, the thin line is the data to be sifted and the thick solid line is the upper envelope constructed by connecting all the local maxima by cubic splines. The original signal has about 64,000 data points and lasts for 640 time units. However, the figure shows only the first six time units of the signal. At the beginning of the signal, one would expect to see an envelope function with zero slope. However, due to the way the cubic splines are constructed, the envelope function exhibits a large swing at the edge of the data. Combined with the similar behavior from the lower envelope, some artificial extrema with relatively large amplitudes are generated. As the sifting procedure is continued, the undesired edge effects can propagate toward the middle of the signal, and eventually corrupt it. Here, a procedure similar to the one in [Huang *et al.*, 1998] is utilized [Yalcinkaya & Lai, 1997; Talcinkaya, 1998] to eliminate the edge effects. Specifically, a number of extra data points is introduced at both the beginning and the end of the data by repeating the local extrema of the typical waves. In order to preserve the original data length, they are located outside the given data interval. As a result, more pairs of additional maxima and minima are to be used by the splines. Figure 15(b) shows the reduction in the artificial swing in the upper envelope function using six extra points at both the beginning and the end of the data.

The edge effects are not the only problems with spline fittings. An ideal envelope should enclose the data and should not interfere with the general flow of it. In reality, however, undershoots and overshoots are present even with very simple data. The example shown in Fig. 15 contains several locations where the envelope crosses the signal and exhibits uncharacteristic swings. It may seem that such imperfections in the envelope construction would have drastic effects in the final form of the intrinsic modes. This turns out not to be the case. In general, the artificial oscillations introduced by the envelopes belong to different time scales, and hence they are eliminated by the sifting procedure.

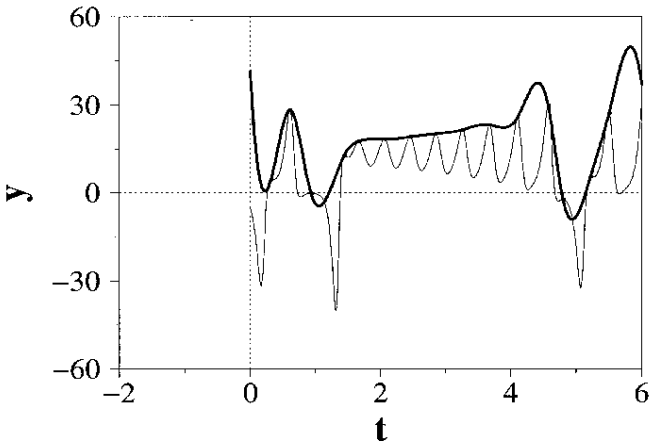

(a)

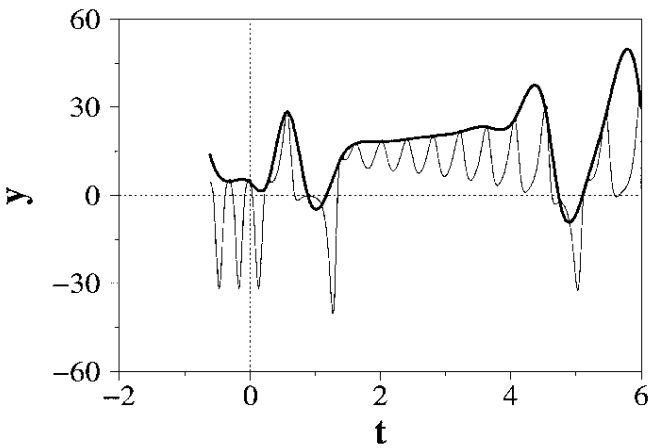

(b)

Fig. 15. (a) A time series collected from the chaotic attractor of the Lorenz system. The upper envelope exhibits a large swing at the beginning of the signal since the edge is not treated. (b) Same data with the edges are properly treated.

Figures 16 and 17 summarize the first seven intrinsic modes from this repeated sifting process with the edge effects taken care of as illustrated in Fig. 15(b). Although it appears that the improvement in the method of spline fitting is critical to minimizing unwanted undulations introduced by the numerical procedure, the choice of which spline to use does not have substantial influence on the obtained intrinsic modes [Yalcinkaya, 1998]. That is, qualitatively similar intrinsic modes are obtained, provided that the splines are smooth functions of time. Therefore, the intrinsic modes, as exemplified in Figs. 16 and 17, are robust.

In general, the number of fundamental modes M required to capture the rotation-like motions in a chaotic signal is *small*. Figure 18 shows the phase functions $\phi_j(t)$ corresponding to the modes shown in Figs. 16 and 17 for the Lorenz flow. There appears to be a separation between the average rotation frequencies (the average slopes) of the various modes, with ω_1 being the largest. It can also be seen that $\omega_j \approx 0$ for $j \geq 7$, indicating that the eighth mode and up are insignificant.

What are the characteristics of the distribution of the mean instantaneous frequencies? Since the signal is chaotic and has a broad-band Fourier spectrum, one may expect an unlocalized distribution of the average frequencies. Nonetheless, as described, the intrinsic modes, by construction, have narrow bandwidth. Therefore, the EMD method yields frequency components that are inherently different from those of Fourier transform. Figure 19 shows the histograms of the average instantaneous frequencies for all three state variables, $x(t)$, $y(t)$ and $z(t)$, of the Lorenz equations with $\sigma = 16$, $\rho = 45.92$ and $\beta = 4$. Each histogram is obtained by using 5000 samples with random initial conditions and calculating $\langle \omega_j \rangle$ for $(j = 1, \ldots, 4)$. There is a clear separation among the distributions of the average frequencies for the intrinsic modes. A quick look at the average of the frequency distributions reveals something more interesting. Table 2 shows the mean of the instantaneous frequency distribution from the x-component of the Lorenz system, the associated standard deviation and the relative ratios. If the mean instantaneous frequency of C_1 is regarded as the fundamental frequency, the remaining intrinsic modes exhibit roughly rational harmonics of this fundamental frequency. A similar relationship can be found in Tables 3 and 4, the corresponding results for $y(t)$ and $z(t)$. Furthermore, $x(t)$ and $y(t)$ seem to have approximately the same frequency distribution and same fundamental frequencies, i.e. $\omega_x \cong \omega_y$. This shows that the phase dynamics of the Lorenz system has an unexpected simplicity. Roughly speaking, there are *only two fundamental frequencies governing the phase dynamics* of the Lorenz equations and all the auxiliary frequencies are obtained from these two.

In principle, an infinitely long chaotic signal can be decomposed into an infinite number of proper rotations. However, we find that the amplitudes and the average rotation frequencies decrease rapidly as higher-order modes are examined. Thus, a few proper rotations are sufficient to represent the phase of the chaotic signal, but there is rigorous assurance of this at the present.

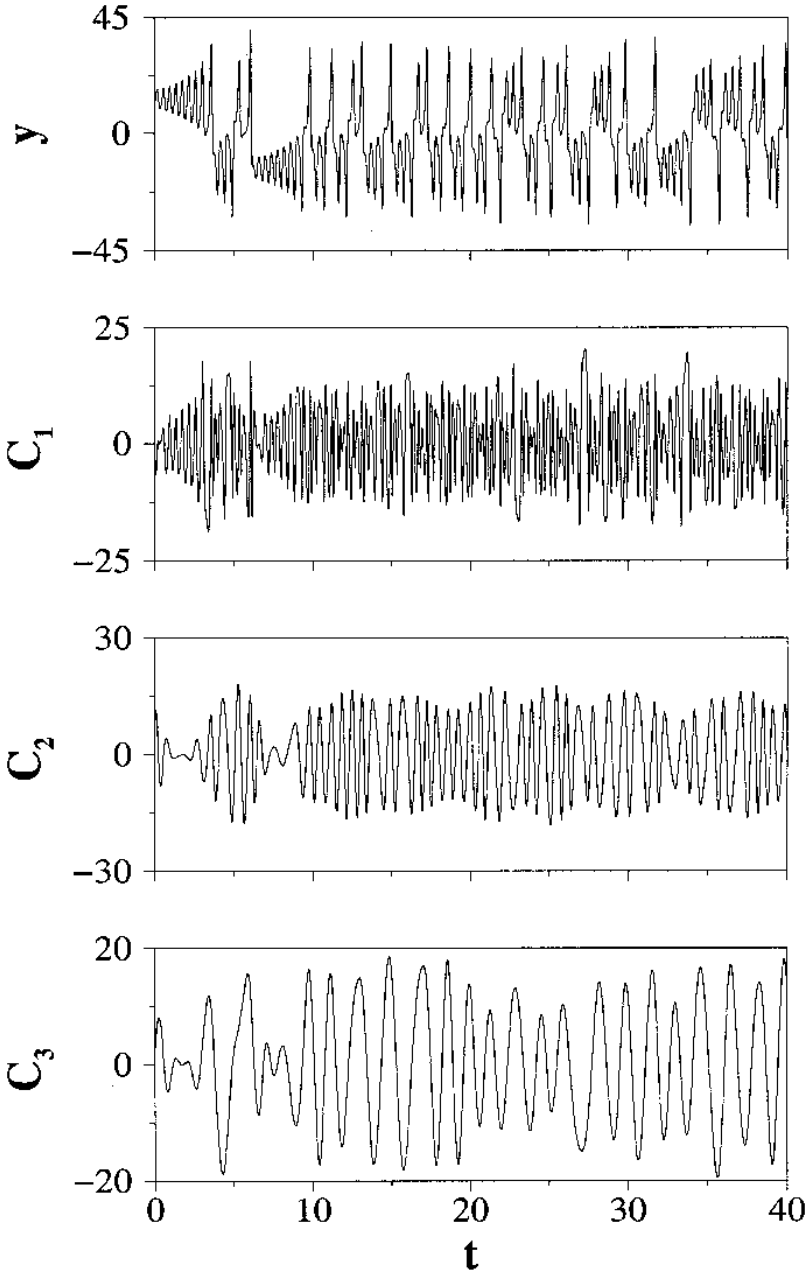

Fig. 16. A trajectory from the y component of the Lorenz equation and the three intrinsic modes.

It should be mentioned that while the sifting procedure is necessary for chaotic flows that exhibit multiple centers of rotation in the complex plane of its analytic signal, there are systems in which the flow apparently already has a unique center of rotation. In this case, the sifting procedure is not necessary and one can define the phase associated with the flow directly from the analytic signal. Flows on the Rössler attractor appear to belong to this category [Rössler, 1976].

3.4. *Application to chaotic systems (II): Transition to chaos in deterministic flows*

A fundamental question in nonlinear science concerns how turbulent or chaotic motions occur as a system parameter changes. About a half century ago, Landau proposed that turbulent motion was a result of successive addition of a great many new discrete frequency components as the system

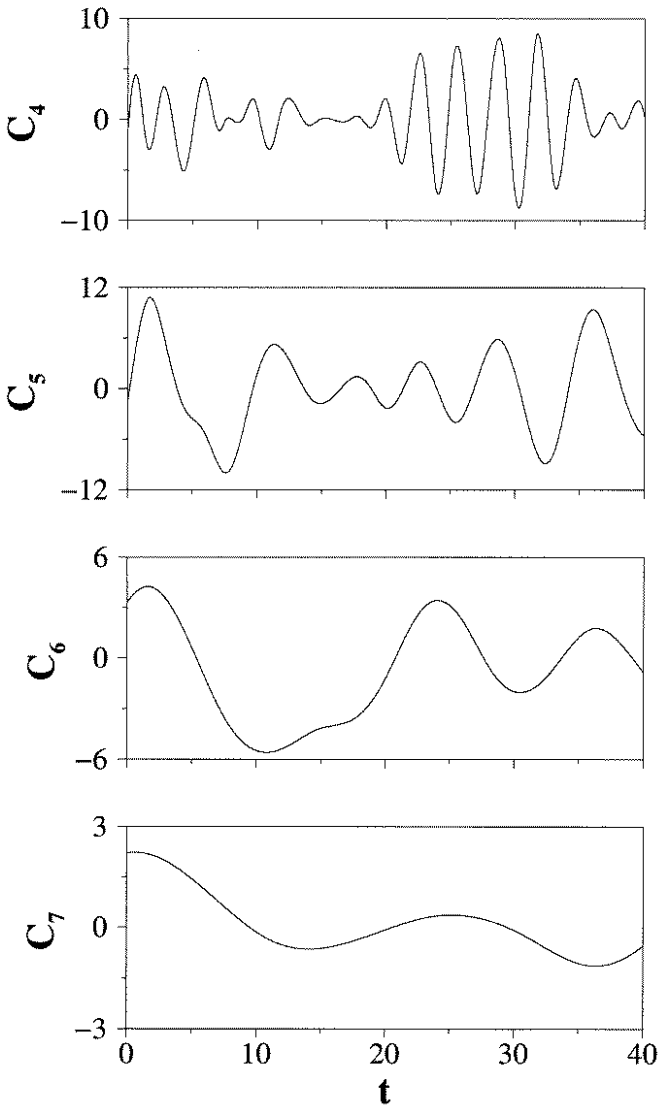

Fig. 17. Next four intrinsic modes from the data shown in 16.

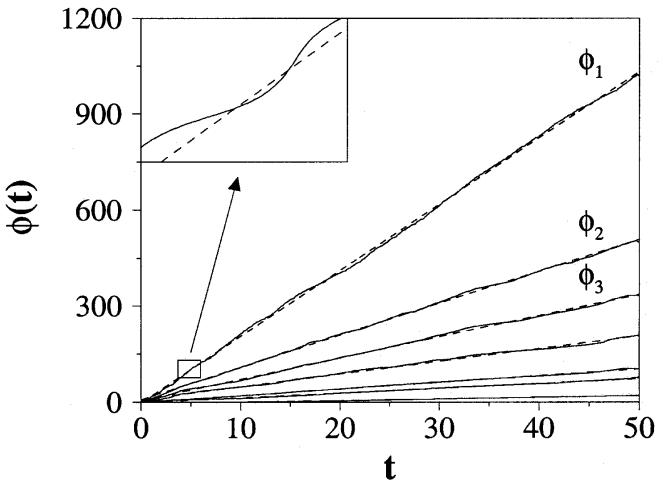

Fig. 18. $\phi_j(t)$ versus t for $j = 1, \ldots, 8$. Note that the phase variation in $\phi_8(t)$ is already approximately zero, indicating that further components are insignificant.

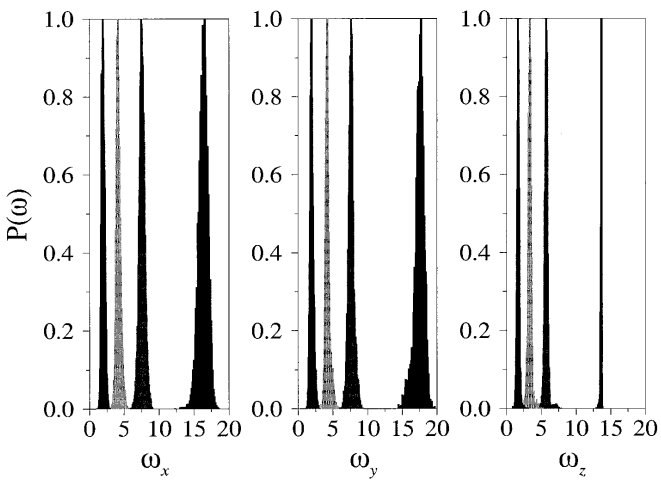

Fig. 19. The histograms obtained from the Lorenz chaotic system. Each distribution is obtained by using 5000 random initial conditions, each yielding a time series for $0 \leq t \leq 600$ (after a sufficiently long transient time). The mean frequencies of the first four intrinsic modes are shown.

parameter approaches the critical point [Landau, 1944] at the onset of the motion.[6] This scenario to turbulence, however, was shown to be incorrect by Ruelle, Takens, and Newhouse who proved mathematical theorems concerning the transition to chaotic motion from four- and three-frequency quasiperiodic flows [Ruelle & Takens, 1971; Newhouse *et al.*, 1978]. In particular, Ruelle and Takens considered four-frequency quasiperiodic flows on the torus T^4. They showed that it is possible to make arbitrarily small, but carefully chosen, smooth perturbations to the flow so that the flow becomes chaotic [Ruelle & Takens, 1971]. Newhouse, Ruelle, and Takens subsequently showed that the same hold for a three frequency quasiperiodic flow on the torus T^3 [Newhouse *et al.*, 1978]. The key implication of these results is that broad-band frequency spectra, a hallmark of turbulent or chaotic motions, can appear more abruptly as the result of the onset of a chaotic attractor. To be more specific, consider a

[6]Here the word *turbulent* means random and complicated motions such as a chaotic motion, as used by Landau [1944].

Table 2. Frequency distribution of x-component from the Lorenz chaotic attractor.

$x(t)$	$\langle\omega\rangle$	σ	ratio
C_1	16.3	0.68	ω_x
C_2	7.6	0.43	$\approx \frac{\omega_x}{2}$
C_3	4.1	0.32	$\approx \frac{\omega_x}{4}$
C_4	1.0	0.24	$\approx \frac{\omega_x}{16}$

Table 3. Frequency distribution of y-component from the Lorenz chaotic attractor.

$y(t)$	$\langle\omega\rangle$	σ	ratio
C_1	17.4	0.71	ω_y
C_2	7.6	0.41	$\approx \frac{\omega_y}{2}$
C_3	4.2	0.31	$\approx \frac{\omega_y}{4}$
C_4	1.9	0.26	$\approx \frac{\omega_y}{8}$

Table 4. Frequency distribution of z-component from the Lorenz chaotic attractor.

$z(t)$	$\langle\omega\rangle$	σ	ratio
C_1	13.6	0.08	ω_z
C_2	5.8	0.28	$\approx \frac{\omega_z}{2}$
C_3	3.4	0.26	$\approx \frac{\omega_z}{4}$
C_4	1.7	0.85	$\approx \frac{\omega_z}{8}$

physical system described by a continuous flow:

$$\frac{d\mathbf{x}}{dt} = \mathbf{F}(\mathbf{x}, p)\,, \tag{56}$$

where $\mathbf{x} \in \mathbf{R}^N$ and p is a system parameter. Assume at $p = p_1$, the flow is quasiperiodic. In this case, if one examines the Fourier spectrum of $\mathbf{x}(t)$, one finds only a few incommensurate Fourier frequencies. According to Ruelle, Takens, and Newhouse, an arbitrarily small change, say in the parameter p from p_1 to $p_2 = p_1 + \delta p$, where $\delta p \sim 0$, can lead to a chaotic motion characterized by a broad-band Fourier spectrum. Note that there is in fact an infinite number of incommensurate Fourier frequencies associated with the chaotic motion at p_2, whereas there are only a very few such frequencies at p_1 even if $|p_2 - p_1| \to 0$. Thus, an infinite number of fundamental Fourier frequencies must have been created through an arbitrarily small parameter change.

The point here is that the transition to chaos in deterministic flows can also be studied from the perspective of analytic signals [Lai, 1998]. Given a scalar time series $x(t)$ from a nonlinear system, one can perform the Hilbert transform to obtain an analytic signal and its instantaneous-frequency spectrum. It is found then [Lai, 1998]: (1) the distributions of the instantaneous frequencies for a chaotic system are typically well localized and exhibit no broad-band feature, in contrast to the Fourier spectra of chaotic signals, and (2) there is no substantial change in the number of analytic signals that constitute a dynamical variable before and after the onset of chaos. Transition to chaos in nonlinear systems can then be considered as a rather smooth process when it is viewed from the perspective of analytic signals rather than the traditional Fourier spectra. These results suggest an interesting organization of chaos in continuous flows, that is, chaos is supported by only a few distinct rotations in the complex representations of analytic signals.

These results can be demonstrated [Lai, 1998] by using a representative model of the two-mode truncation of the complex coefficient Ginzburg–Landau equation. The model represents a four-dimensional autonomous flow [Moon, 1997], as follows:

$$\begin{aligned}\frac{da_1}{dt} &= pa_1 + (i-p)\left(|a_1|^2 a_1 + a_1|a_2|^2 + \frac{1}{2}a_1^* a_2^2\right)\,,\\ \frac{da_2}{dt} &= pa_2 - q^2(i+p)a_2 + (i-p)\\ &\quad\times\left(a_1^2 a_2^* + 2|a_1|^2 a_2 + \frac{3}{4}|a_2|^2 a_2\right),\end{aligned} \tag{57}$$

where $a_1(t)$ and $a_2(t)$ are complex dynamical variables, the star denotes complex conjugate, p and q are parameters. It was argued that Eq. (57) exhibits a transition from two-frequency quasiperiodic motion to chaos in wide parameter regimes via the mechanism of heteroclinic crossing of stable and unstable manifolds and torus breakup [Moon, 1997]. In fact, a two-frequency quasiperiodic motion can lose its stability directly and become chaotic. In

[Lai, 1998], the parameter q is fixed at $q = 1.0$ and the following notions are used: $U(t) \equiv \mathrm{Re}[a_1(t)]$, $V(t) \equiv \mathrm{Im}[a_1(t)]$, $X(t) \equiv \mathrm{Re}[a_2(t)]$, and $Y(t) \equiv \mathrm{Im}[a_2(t)]$. Numerical compuation indicates that the transition from two-frequency quasiperiodicity to chaos occurs at the critical parameter value $0.24 < p_c < 0.25$, where the motion is quasiperiodic for $p > p_c$ and it is chaotic for $p < p_c$. Figure 20(a) shows, for $p = 0.25$, the projection of the quasiperiodic attractor (after a transient time of $t = 50\,000$) onto the (U, X) plane, and Fig. 20(b) shows the Fourier power spectrum of $U(t)$ for $0 \leq t \leq 3276.8$ at a sampling rate $\Delta t = 0.05$ (so that there are 2^{16} points in the time series for fast Fourier transform). The Fourier spectrum is apparently discrete and there are two fundamental frequencies [Moon, 1997]. As p decreases, the two-frequency torus in which the quasiperiodic attractor lies breaks at p_c, and the asymptotic attractor becomes chaotic with a fractal dimension between 3 and 4 for $p < p_c$ [Moon, 1997]. Figures 20(c) and 20(d) show the projection of the chaotic attractor in the (U, X) plane and the Fourier power spectrum of $U(t)$, respectively. Clearly, the Fourier spectrum now has a broad-band feature, which is a hallmark of chaos. Comparison between Figs. 20(b) and 20(d) indicates that an infinite number of new Fourier modes are created at the onset of chaos.

To study the transition to chaos, as demonstrated in Figs. 20(a)–20(d), from the standpoint of

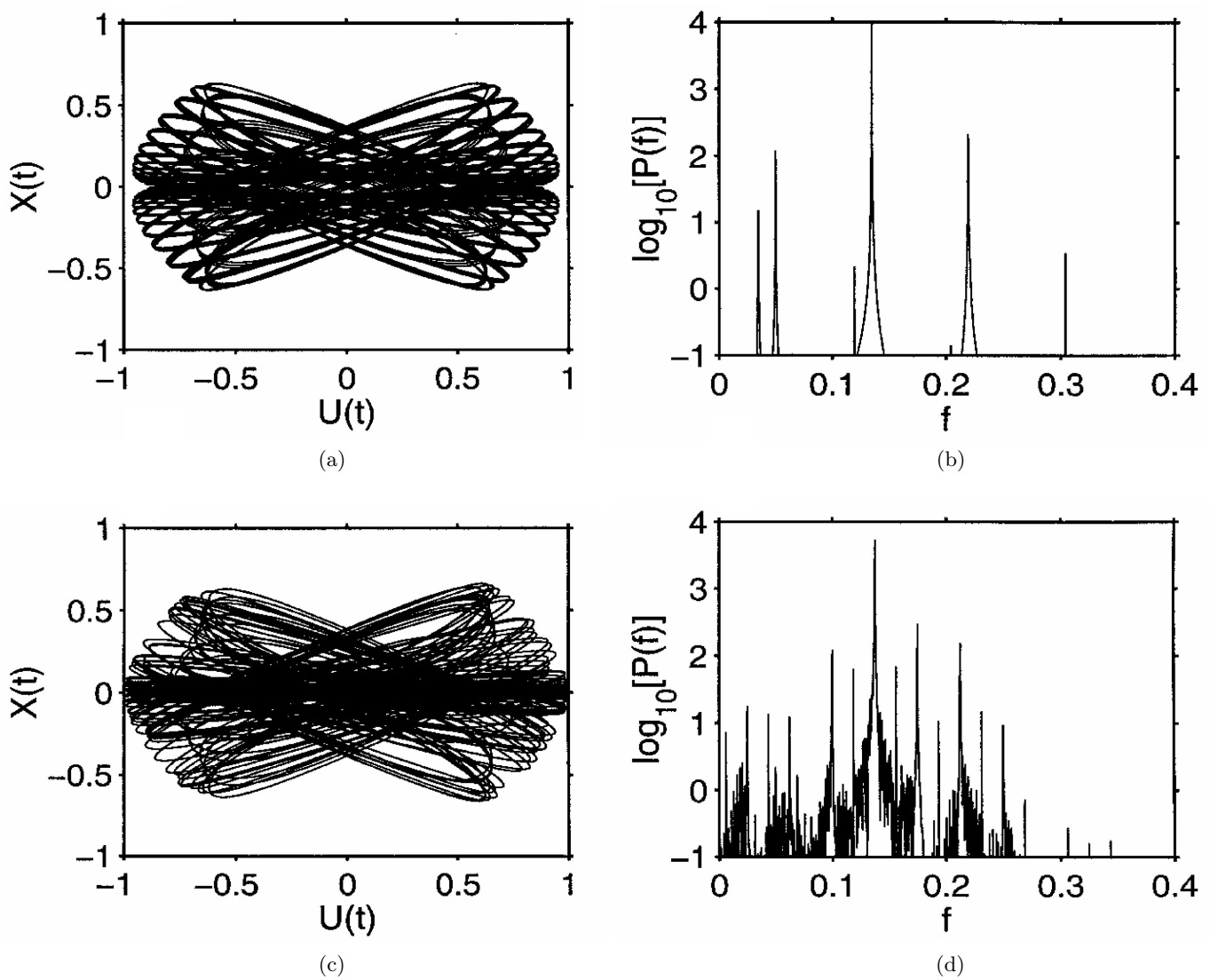

Fig. 20. (a) For $p = 0.25$ (two-frequency quasiperiodicity), a trajectory in the (U, X) plane. (b) The Fourier spectrum of $U(t)$ in (a). (c) For $p = 0.24$ (chaos), a trajectory in the (U, X) plane. (d) The Fourier spectrum of $U(t)$ in (c).

analytic signals, it is necessary to decompose a time series into empirical modes with proper rotational structures. One can then obtain quantitative characteristics of the rotations from the analytic signal of each component by utilizing the Hilbert transform. This has been done for both the quasiperiodic and chaotic motions in Eq. (57) by decomposing the time series $U(t)$ into components with proper analytic signals: $U(t) = \sum_{i=1}^{M} C_i(t)$, where M is the number of modes with nonzero mean frequencies of rotation. For a time series of 2^{16} points at a sampling rate of $\Delta t = 0.05$, it is found [Lai, 1998] that $M \approx 6$ suffices to capture the time variation of the original signal $U(t)$. Figures 21(a) and 21(b) show, for $p = 0.25$, the first two rotations in the complex planes of their own analytic signals. The average frequencies of these two rotations are $\omega_1 \approx 0.846$ and $\omega_2 \approx 0.314$, respectively. The rotations reveal rather regular patterns, as can be expected for a quasiperiodic motion. As p decreases through p_c so that the system is in a chaotic regime, these proper analytic signals still persist. Figures 21(c) and 21(d) show the corresponding rotations for $p = 0.24$. Due to chaos, the rotations no longer exhibit regular patterns, but the overall behaviors of rotation persist. The average frequencies of rotation are $\omega_1 \approx 0.864$ and $\omega_2 \approx 0.378$ for modes 1 and 2, respectively. We see that the mean frequency of the first

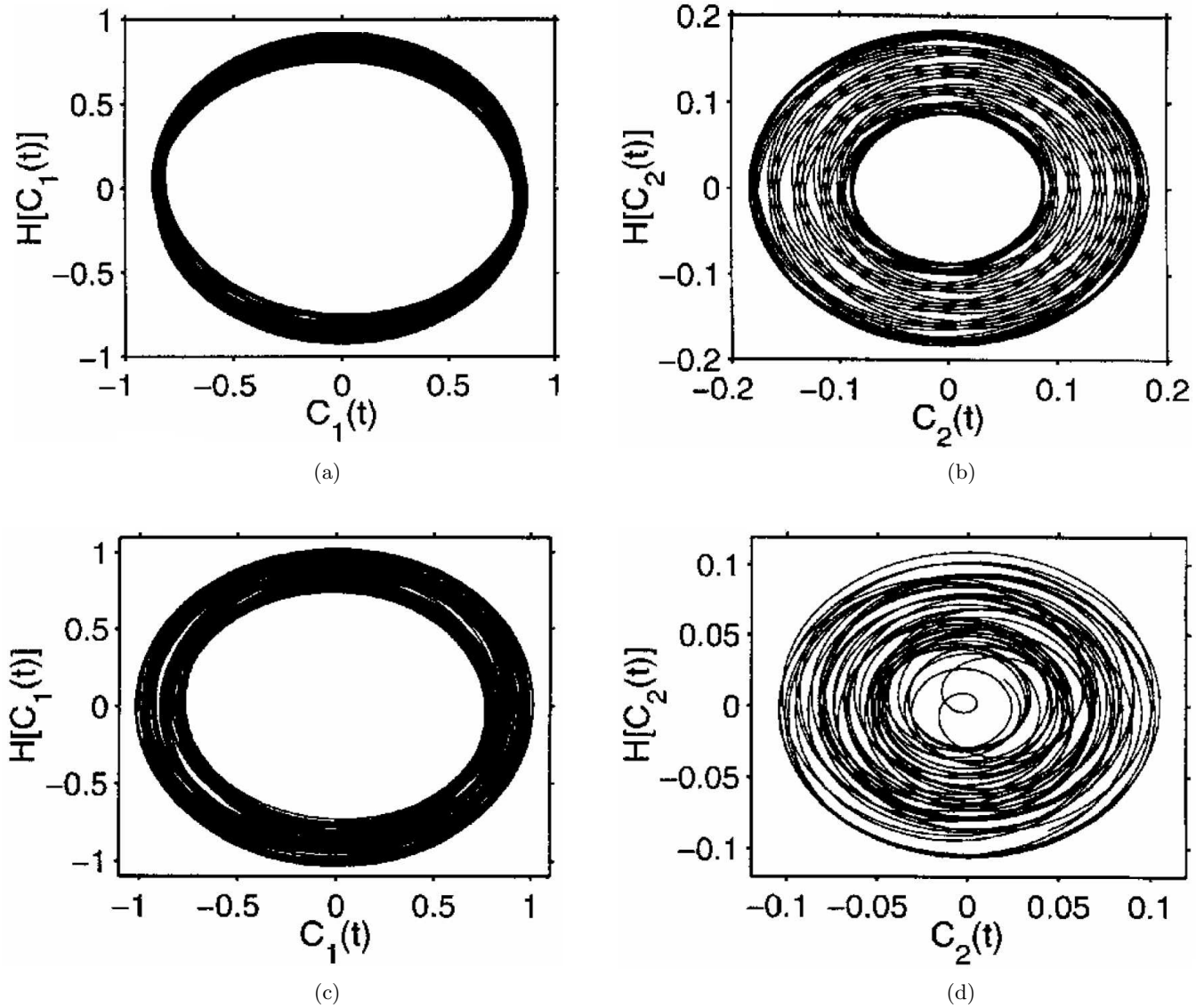

Fig. 21. The first two proper analytic signals obtained from $U(t)$. (a) $p = 0.25$ (quasiperiodicity), mode 1; (b) $p = 0.25$ (quasiperiodicity), mode 2; (c) $p = 0.24$ (chaos), mode 1; and (d) $p = 0.24$ (chaos), mode 2.

analytic signal changes only slightly as p decreases from 0.25 to 0.24, and the corresponding change in the second analytic signal is rather large. In general, it is observed [Lai, 1998] that the onset of chaos usually has a greater influence on rotations with smaller frequencies.

The remarkable result is that as the quasiperiodic motion is converted into a chaotic one, the number of proper analytic signals characterizing a chaotic signal remains essentially the same. For instance, it is found that the chaotic signal $U(t)$ in Fig. 20(c) can still be represented by six proper analytic signals [Lai, 1998]. One way to examine the change in proper analytic signals for quasiperiodic and chaotic signals is to study the statistical behavior of mean frequencies of rotation. Specifically, in [Lai, 1998], for a fixed parameter value p, 10 000 trajectories (each of 2^{16} points, at a sampling rate $\Delta t = 0.05$) are chosen on the attractor and for each trajectory, the mean frequencies of the first six modes of proper rotations are computed. The histograms of these six frequencies $(\omega_1, \ldots, \omega_6)$ are then constructed. Figures 22(a) and 22(b) show the histograms for $p = 0.25$ and $p = 0.24$, respectively. When the motion is quasiperiodic [Fig. 3(a)], it can be seen that the first few frequencies are sharply distributed. In fact, some of the frequencies are the linear combinations of others, which occurs commonly in the Fourier analysis. For instance, it is found that $\omega_3 \approx (\omega_2 + \omega_4)/2$ [Lai, 1998]. For the chaotic motion [Fig. 3(b)], the frequencies *spread* and the frequency distributions shift relative to those in the quasiperiodic case. However, the first few frequency distributions in the chaotic case are still well localized. One important feature distinguishing a chaotic rotation from a regular one is that for a chaotic rotation: $\psi(t) = A(t) \exp[i\phi(t)]$, the amplitude $A(t)$ is random and the phase dynamics are similar to a random walk. This is due to the fact that the phase dynamics can be described by: $d\phi(t)/dt = \omega + F[A(t)]$, where $F[A(t)]$ is a function of $A(t)$ [Rosenblum *et al.*, 1996; Yalcinkaya & Lai, 1997; Andrade *et al.*, 2000; Andrade & Lai, 2001]. The most important feature of Figs. 3(a) and 3(b) is

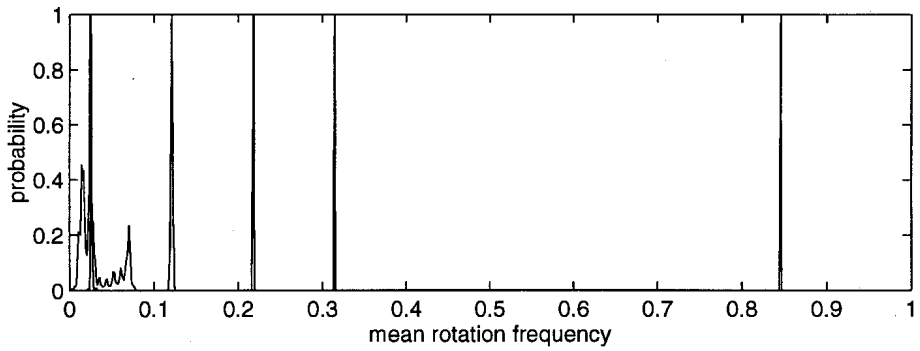

(a) $p = 0.25$

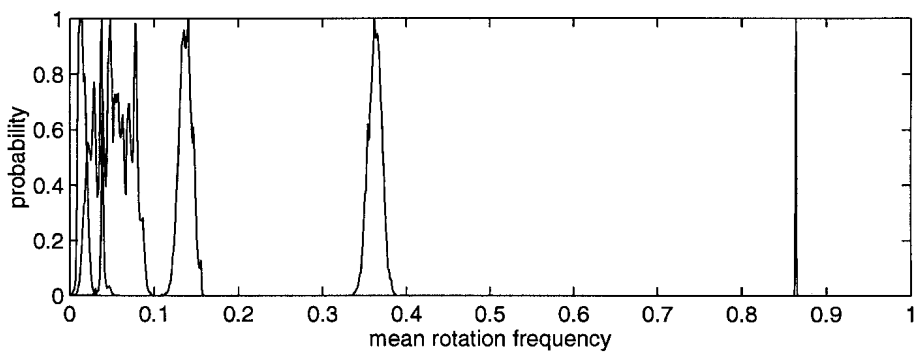

(b) $p = 0.24$

Fig. 22. Histograms of mean frequencies of proper analytic signals associated with the $U(t)$ for (a) the quasiperiodic motion at $p = 0.25$ and (b) for the chaotic motion at $p = 0.24$.

that the number of proper analytic signals remains essentially unchanged through the transition from quasiperiodicity to chaos, and the distributions of the instantaneous frequencies of the analytic signals are *well localized* and exhibit no broad-band feature. A reason may be that in the rotational representation, the chaotic amplitude modulation is filtered out so that the broad-band component in the Fourier spectrum disappears.[7] Thus, although an infinite number of Fourier modes are created at the onset of chaos, there is no metamorphosis in the number of analytic signals that represent a chaotic time series.

A few remarks are in order. The frequencies ω_j obtained correspond to the mean rotation frequencies of the empirical modes $C_j(t)$ $(j = 1, \ldots, M)$ in the complex planes of their analytic signals. These frequencies, in fact, characterize the main physical time scales hidden in the original time series $U(t)$ *from the perspective of rotations*. The frequencies ω_j can be rationally related and there are only two incommensurate ones, which are consistent with the fact that the underlying flow is two-frequency quasiperiodic. The Fourier frequencies, on the other hand, are harmonic frequencies. When the motion is regular, the fundamental frequencies in the analytic-signal representation correspond approximately to these in the Fourier representation, or the "real" frequencies of the quasiperiodic motion [compare Figs. 20(b) and 22(a)]. When the motion is chaotic, the Fourier spectrum is broad-band, but the frequency distribution in the analytic-signal representation is still well localized, due to the fact that there cannot be abrupt change in the analytic signals (rotations) that constitute the physical signal. In this case, there is no direct correspondence between the rotation frequencies of the analytic signals and the Fourier frequencies.

4. Discussion

In this paper we have described two recent developments in chaotic time series analysis: (1) the delay-coordinate embedding method for analyzing transient chaotic data and, (2) the Hilbert-transform method for chaotic signal processing. The first extends the embedding method, proven to be useful for long time series from low-dimensional chaotic systems, to systems that exhibit transient chaos and consequently give only short time series. The second can be applied to both deterministic and stochastic systems. In addition, the Hilbert analysis has the advantage of being suitable for nonstationary time series to assess the instantaneous-frequency spectrum of the system.

When combined with the empirical-mode decomposition procedure, the Hilbert transform can yield an understanding of the physical mechanisms responsible for the observed time series, which cannot be revealed by the traditional Fourier or the wavelet transform method. An example is the record of the time of a day. The exact time of a day on earth is not precisely 24 hours. Instead, the time has fluctuations on the order of microseconds. By analyzing the data of fluctuations using the empirical-mode decomposition and the Hilbert analysis, Huang *et al.* were able to identify clearly the physical origins of the fluctuations such as the influences from the motions of the sun and the moon, as these physical motions have distinct instantaneous-frequency properties [Huang *et al.*, 1998].

The analytic-signal approach can also be utilized to address fundamental questions in chaotic dynamics such as the transition to chaos in deterministic flows. For instance, a study of the rotational characteristics of the analytic signals suggests that there is no significant change in the number of proper analytic signals through the transition, although the Fourier spectrum becomes broad-band after the onset of chaos. Thus, although chaotic motion can be characterized as random and complicated, its fundamental structure in terms of proper analytic signals may be quite simple.

Acknowledgments

This work is supported by AFOSR under Grant No. F49620-01-1-0317. Part of the materials in the Hilbert analysis is based on part of the Ph.D. thesis by T. Yalcinkaya at the University of Kansas in 1998 under Y. C. Lai.

[7]By filtering out the chaotic amplitude modulations, the organization of the phase dynamics, which is characterized by the rotation frequencies, becomes quite simple in the sense that the distributions of frequencies are well isolated [Fig. 22(b)] even in chaotic regimes. A somewhat analogous situation occurs in the periodic-orbit representation of chaotic sets. It is believed that the infinite set of unstable periodic orbits constitutes the skeleton of a chaotic set. In this sense, chaos can be regarded as being organized on the infinite set of periodic orbits, but apparantly, there is a even larger set of *aperiodic* orbits embedded in the set. In our case, by focusing on the rotational characteristics of a chaotic flow, its organization becomes simple.

References

Abarbanel, H. D. I. [1996] *Analysis of Observed Chaotic Data* (Springer, NY).

Allie, S. & Mees, A. [1997] "Finding periodic points from short time series," *Phys. Rev.* **E56**, 346–350.

Andrade, V., Davidchack, R. L. & Lai, Y.-C. [2000] "Noise scaling in phase synchronization of coupled chaotic oscillators," *Phys. Rev.* **E61**, 3230–3233.

Andrade, V. & Lai, Y.-C. [2001] "Super persistent chaotic transients in physical systems: Effect of noise on phase synchronization of coupled chaotic oscillators," *Int. J. Bifurcation and Chaos* **11**, 2607–2619.

Arfken, G. B. & Weber, H. J. [1995] *Mathematical Methods for Physicists* (Academic Press, San Diego).

Auerbach, D., Cvitanovic, P., Eckmann, J.-P., Gunaratne, G. H. & Procaccia, I. [1987] "Exploring chaotic motion through periodic orbits," *Phys. Rev. Lett.* **58**, 2387–2389.

Badii, R., Brun, E., Finardi, M., Flepp, L., Holzner, R., Pariso, J., Reyl, C. & Simonet, J. [1994] "Progress in the analysis of experimental chaos through periodic orbits," *Rev. Mod. Phys.* **66**, 1389–1415.

Bedrosian, E. [1963] "A product theorem for Hilbert transform," *Proc. IEEE* **51**, 868–869.

Benettin, G., Galgani, L., Giorgilli, A. & Strelcyn, J. M. [1980] "Lyapunov characteristic exponents for smooth dynamical systems and for Hamiltonian systems: A method for computing all of them. Part 2: Numerical application," *Meccanica* **15**, p. 21.

Biham, O. & Wenzel, W. [1989] "Characterization of unstable periodic orbits in chaotic attractors and repellers," *Phys. Rev. Lett.* **63**, 819–822.

Boashash, B. [1992] "Estimating and interpreting the instantaneous frequency of a signal, I. Fundamentals," *Proc. IEEE* **80**, 520–538.

Boashash, B., Powers, E. J. & Zoubir, A. M. [1995] *Higher-Order Statistical Signal Processing* (J. Wiley, NY).

Boccaletti, S., Grebogi, C., Lai, Y.-C., Mancini, H. & Maza, D. [2000] "Control of chaos: Theory and applications," *Phys. Rep.* **329**, 103–197.

Brown, R., Bryant, P. & Abarbanel, H. D. I. [1991] "Computing the Lyapunov spectrum of a dynamical system from an observed time series," *Phys. Rev.* **A43**, 2787–2806.

Buzug, T. & Pfister, G. [1992] "Optimal delay time and embedding dimension for delay-time coordinates by analysis of the glocal static and local dynamic behavior of strange attractors," *Phys. Rev.* **A45**, 7073–7084.

Chan, Y. T. [1995] *Wavelet Basics* (Kluwer, Boston).

Chen, Q., Ott, E. & Hurd, L. P. [1991] "Calculating topological entropies of chaotic dynamical systems," *Phys. Lett.* **A156**, 48–52.

Chen, G. [1999] *Controlling Chaos and Bifurcations in Engineering Systems* (CRC Press, Boca Raton, FL).

Christini, D. J. & Collins, J. J. [1995] "Controlling nonchaotic neuronal noise using chaos control techniques," *Phys. Rev. Lett.* **75**, 2782–2785.

Davidchack, R. L. & Lai, Y. C. [1999] "Efficient algorithm for detecting unstable periodic orbits in chaotic systems," *Phys. Rev.* **E60**, 6172–6175.

Davidchack, R. L., Lai, Y.-C., Bollt, E. M. & Dhamala, M. [2000] "Estimating generating partitions of chaotic systems by unstable periodic orbits," *Phys. Rev.* **E61**, 1353–1356.

Davidchack, R. L., Lai, Y.-C., Klebanoff, A. & Bollt, E. M. [2001] "Towards complete detection of unstable periodic orbits in chaotic systems," *Phys. Lett.* **A287**, 99–104.

Dawson, S., Grebogi, C., Sauer, T. D. & Yorke, J. A. [1994] "Obstructions to shadowing when a Lyapunov exponent fluctuates about zero," *Phys. Rev. Lett.* **73**, 1927–1930.

Dhamala, M., Lai, Y.-C. & Kostelich, E. J. [2000] "Detecting unstable periodic orbits from transient chaotic time series," *Phys. Rev.* **E61**, 6485–6489.

Dhamala, M., Lai, Y.-C. & Kostelich, E. J. [2001] "Analysis of transient chaotic time series," *Phys. Rev.* **E64**, 056207(1–9).

Ding, M., Grebogi, C., Ott, E., Sauer, T. D. & Yorke, J. A. [1993] "Plateau onset for correlation dimension: When does it occur?" *Phys. Rev. Lett.* **70**, 3872–3875.

Eckmann, J.-P. & Ruelle, D. [1985] "Ergodic theory of chaos and strange attractors," *Rev. Mod. Phys.* **57**, 617–656.

Eckmann, J.-P., Kamphorst, S. O., Ruelle, D. & Ciliberto, S. [1986] "Lyapunov exponents from time series," *Phys. Rev.* **A34**, 4971–4979.

Farmer, J. D., Ott, E. & Yorke, J. A. [1983] "The dimension of chaotic attractors," *Physica* **D7**, 153–180.

Frenking, M. E. [1994] *Digital Signal Processing in Communication Systems* (Van Nostrand Reinhold, NY).

Gabor, D. [1946] "Theory of communication," *J. IEE Lond.* **93**, 429–457.

Garfinkel, A., Spano, M. L., Ditto, W. L. & Weiss, J. N. [1992] "Controlling cardiac chaos," *Science* **257**, 1230–1233.

Goodridge, C. L., Pecora, L. M., Carroll, T. L. & Rachford, F. J. [2001] "Detecting functional relationships between simultaneous time series," *Phys. Rev.* **E64**, 026221.

Grassberger, P. & Procaccia, I. [1983a] "Characterization of strange attractors," *Phys. Rev. Lett.* **50**, 346–348.

Grassberger, P. & Procaccia, I. [1983b] "Measuring the strangeness of strange attractors," *Physica* **D9**, 189–208.

Grassberger, P. & Kantz, H. [1985] "Repellers, semi-attractors, and long-lived chaotic transients," *Physica* **D17**, 75–86.

Grebogi, C., Ott, E. & Yorke, J. A. [1982] "Chaotic attractors in crisis," *Phys. Rev. Lett* **48**, 1507–1510.

Grebogi, C., Ott, E. & Yorke, J. A. [1983] "Crises, sudden changes in chaotic attractors and chaotic transients," *Physica* **D7**, 181–200.

Grebogi, C., Ott, E. & Yorke, J. A. [1988] "Unstable periodic orbits and the dimensions of multifractal chaotic attractors," *Phys. Rev.* **A37**, 1711–1724.

Grebogi, C., Hammel, S. M., Yorke, J. A. & Sauer, T. D. [1990] "Shadowing of physical trajectories in chaotic dynamics: Containment and refinement," *Phys. Rev. Lett.* **65**, 1527–1530.

Gunaratne, G. H. & Procaccia, I. [1987] "Organization of chaos," *Phys. Rev. Lett.* **59**, 1377–1380.

Hahn, S. L. [1996] *Hilbert Transforms in Signal Processing* (Artech House, Boston).

Hammel, S. M., Yorke, J. A. & Grebogi, C. [1987] "Do numerical orbits of chaotic dynamical processes represent true orbits?" *J. Complexity* **3**, 136–145.

Hammel, S. M., Yorke, J. A. & Grebogi, C. [1988] "Numerical orbits of chaotic processes represent true orbits," *Bull. Am. Math. Soc.* **19**, 465–469.

Hénon, M. [1976] "A two-dimensional mapping with a strange attractor," *Commun. Math. Phys.* **50**, 69–76.

Hsu, G.-H., Ott, E. & Grebogi, C. [1988] "Strange saddles and the dimensions of their invariant manifolds," *Phys. Lett.* **A127**, 199–204.

Huang, N. E., Shen, Z., Long, S. R., Wu, M. C., Shih, H. H., Zheng, Q., Yen, N. C., Tung, C. C. & Liu, H. H. [1998] "The empirical mode decomposition and the Hilbert spectrum for nonlinear and non-stationary time series," *Proc. R. Soc. Lond.* **A454**, 903–995.

Hunt, B. R., Ott, E. & Yorke, J. A. [1996] "Fractal dimensions of chaotic saddles of dynamical systems," *Phys. Rev.* **E54**, 4819–4823.

Jacobs, J., Ott, E. & Grebogi, C. [1997] "Computing the measure of nonattracting chaotic sets," *Physica* **D108**, 1–11.

Janosi, I. M. & Tél, T. [1994] "Time-series analysis of transient chaos," *Phys. Rev.* **E49**, 2756–2763.

Jones, S. W. & Aref, H. [1988] "Chaotic advection in pulsed-source sink systems," *Phys. Fluids* **31**, 469–485.

Jones, S. W., Thomas, O. & Aref, H. [1989] "Chaotic advection by laminar-flow in a twisted pipe," *J. Fluid. Mech.* **209**, 335–357.

Jung, C. & Ziemniak, E. [1992] "Hamiltonian scattering chaos in a hydrodynamical system," *J. Phys. A Math. Gen.* **25**, 3929–3943.

Jung, C., Tél, T. & Ziemniak, E. [1993] "Application of scattering chaos to particle transport in hydrodynamical flow," *Chaos* **3**, 555–568.

Kantz, H. & Schreiber, T. [1997] *Nonlinear Time Series Analysis* (Cambridge University Press, Cambridge, UK).

Karolyi, G. & Tél, T. [1997] "Chaotic tracer scattering and fractal basin boundaries in a blinking vortex-sink system," *Phys. Rep.* **290**, 125–147.

Károlyi, G., Péntek, A., Toroczkai, Z., Tél, T. & Grebogi, C. [1999] "Chemical or biological activity in open chaotic flows," *Phys. Rev.* **E59**, 5468–5481.

Kember, G. & Fowler, A. C. [1993] "A correlation-function for choosing time delays in-phase portrait reconstructions," *Phys. Lett.* **A179**, 72–80.

Lai, Y.-C., Grebogi, C., Yorke, J. A. & Kan, I. [1993] "How often are chaotic saddles nonhyperbolic?" *Nonlinearity* **6**, 779–797.

Lai, Y.-C., Lerner, D. & Hayden, R. [1996] "An upper bound for the proper delay time in chaotic time series analysis," *Phys. Lett.* **A218**, 30–34.

Lai, Y.-C. [1997] "Characterization of the natural measure by unstable periodic orbits in nonhyperbolic chaotic systems," *Phys. Rev.* **56**, 6531–6539.

Lai, Y.-C., Nagai, Y. & Grebogi, C. [1997] "Characterization of the natural measure by unstable periodic orbits in chaotic attractors," *Phys. Rev. Lett.* **79**, 649–652.

Lai, Y.-C. [1998] "Analytic signals and the transition to chaos in deterministic flows," *Phys. Rev.* **E58**, R6911–R6914.

Lai, Y.-C. & Lerner, D. [1998] "Effective scaling regime for computing the correlation dimension in chaotic time series analysis," *Physica* **D115**, 1–18.

Lai, Y.-C. & Grebogi, C. [1999] "Modeling of coupled chaotic oscillators," *Phys. Rev. Lett.* **82**, 4803–4806.

Lai, Y.-C., Grebogi, C. & Kurths, J. [1999a] "Modeling of deterministic chaotic systems," *Phys. Rev.* **E59**, 2907–2910.

Lai, Y.-C., Lerner, D., Williams, K. & Grebogi, C. [1999b] "Unstable dimension variability in coupled chaotic oscillators," *Phys. Rev.* **E60**, 5445–5454.

Landau, L. D. [1944] "On the problem of turbulence," *C. R. Acad. Sci. USSR* **44**, 311–315.

Lathrop, D. P. & Kostelich, E. J. [1989] "Characterization of an experimental strange attractor by periodic orbits," *Phys. Rev.* **A40**, 4028–4031.

Liebert, W. & Schuster, H. G. [1989] "Proper choice of the time-delay for the analysis of chaotic time-series," *Phys. Lett.* **A142**, 107–111.

Liebert, W., Pawelzik, K. & Schuster, H. G. [1991] "Optimal embeddings of chaotic attractors from topological considerations," *Europhys. Lett.* **14**, 521–526.

Lorenz, E. N. [1963] "Deterministic nonperiodic flow," *J. Atmos. Sci.* **20**, 130–141.

McDonald, S. W., Grebogi, C., Ott, E. & Yorke, J. A. [1985] "Fractal basin boundaries," *Physica* **D17**, 125–153.

Mindlin, G. B., Hou, X.-J., Solari, H. G., Gilmore, R. & Tufillaro, N. B. [1990] "Classification of strange attractors by integers," *Phys. Rev. Lett.* **64**, 2350–2353.

Moon, H.-T. [1997] "Two-frequency motion to chaos

with fractal dimension $d > 3$," *Phys. Rev. Lett.* **79**, 403–406.

Morita, T., Hata, H. Mori, H., Horita, T. & Tomita, K. [1987] "On partial dimensions and spectra of singularities of strange attractors," *Prog. Theor. Phys.* **78**, 511–515.

Newhouse, S., Ruelle, D. & Takens, F. [1978] "Occurrence of strange axiom-a attractors near quasiperiodic flows on t^m, m is greater than or equal to 3," *Commun. Math. Phys.* **64**, 35–40.

Nishikawa, T., Toroczkai, Z., Grebogi, C. & Tél, T. [2002] "Finite-size effects on active chaotic advection," *Phys. Rev.* **E65**, 026216.

Nusse, H. E. & Yorke, J. A. [1989] "A procedure for finding numerical trajectories on chaotic saddles," *Physica* **D36**, 137–156.

Okunev, Y. [1997] *Phase and Phase-Difference Modulation in Digital Communications* (Artech House, Boston).

Ott, E., Grebogi, C. & Yorke, J. A. [1990] "Controlling chaos," *Phys. Rev. Lett.* **64**, 1196–1199.

Ott, E. [1993] *Chaos in Dynamical Systems* (Cambridge University Press, Cambridge, UK).

Packard, N. H., Crutchfield, J. P., Farmer, J. D. & Shaw, R. S. [1980] "Geometry from a time series," *Phys. Rev. Lett.* **45**, 712–716.

Pawelzik, K. & Schuster, H. G. [1991] "Unstable periodic orbits and prediction," *Phys. Rev.* **A43**, 1808–1812.

Pecora, L. M., Carroll, T. L. & Heagy, J. F. [1995] "Statistics for mathematical properties of maps between time series embeddings," *Phys. Rev.* **E52**, 3420–3439.

Pecora, L. M. & Carroll, T. L. [1996] "Discontinuous and nondifferentiable functions and dimension increase induced by filtering chaotic data," *Chaos* **6**, 432–439.

Pecora, L. M., Carroll, T. L. & Heagy, J. F. [1997] "Statistics for continuity and differentiability: An application to attractor reconstruction from time series," *Fields Inst. Commun.* **11**, 49–62.

Pecora, L. M. & Carroll, T. L. [2000] "Detecting chaotic drive-response geometry in generalized synchronization," *Int. J. Bifurcation and Chaos* **10**, 875–889.

Pei, X. & Moss, F. [1996a] "Characterization of low-dimensional dynamics in the crayfish caudal photoreceptor," *Nature* **379**, 618–621.

Pei, X. & Moss, F. [1996b] "Detecting low dimensional dynamics in biological experiments," *Int. J. Neural Syst.* **7**, 429–435.

Pei, X., Dolan, K., Moss, F. & Lai, Y.-C. [1998] "Counting unstable periodic orbits in noisy chaotic systems: A scaling relation connecting experiment with theory," *Chaos* **8**, 853–860.

Péntek, A., Toroczkai, Z., Tél, T., Grebogi, C. & Yorke, J. A. [1995] "Fractal boundaries in open hydrodynamical flows: Signatures of chaotic saddles," *Phys. Rev.* **E51**, 4076–4088.

Pierson, D. & Moss, F. [1995] "Detecting periodic unstable points in noisy chaotic and limit-cycle attractors with applications to biology," *Phys. Rev. Lett.* **75**, 2124–2127.

Pingel, D., Schmelcher, P. & Diakonos, F. K. [2001] "Detecting unstable periodic orbits in chaotic continuous-time dynamical systems," *Phys. Rev.* **E64**, 026214.

Press, W. H., Flannery, B. P., Teukolsky, S. A. & Vetterling, W. T. [1986] *Numerical Recipe* (Cambridge University Press, Cambridge, UK).

Rosenblum, M. G., Pikovsky, A. S. & Kurths, J. [1996] "Phase synchronization of chaotic oscillators," *Phys. Rev. Lett.* **76**, 1804–1807.

Rosenstein, M. T., Collins, J. J. & De Luca, C. J. [1994] "Reconstruction expansion as a geometry-based framework for choosing proper delay times," *Physica* **D73**, 82–98.

Rössler, O. E. [1976] "Equation for continuous chaos," *Phys. Lett.* **A57**, 397–398.

Ruelle, D. & Takens, F. [1971] "Nature of turbulence," *Commun. Math. Phys.* **20**, 167.

Sano, M. & Sawada, Y. [1985] "Measurement of the Lyapunov spectrum from a chaotic time series," *Phys. Rev. Lett.* **55**, 1082–1085.

Sauer, T. D., Yorke, J. A. & Casdagli, M. [1991] "Embedology," *J. Stat. Phys.* **65**, 579–616.

Sauer, T. D., Tempkin, J. A. & Yorke, J. A. [1998] "Spurious Lyapunov exponents in attractor reconstruction," *Phys. Rev. Lett.* **81**, 4341–4344.

Sauer, T. D. & Yorke, J. A. [1999] "Reconstructing the Jacobian from data with observational noise," *Phys. Rev. Lett.* **83**, 1331–1334.

Schiff, S. J., Jerger, K., Duong, D. H., Chang, T., Spano, M. L. & Ditto, W. L. [1994] "Controlling chaos in the brain," *Nature* **370**, 615–620.

Schmelcher, P. & Diakonos, F. K. [1997] "Detecting unstable periodic orbits of chaotic dynamical systems," *Phys. Rev. Lett.* **78**, 4733–4736.

Schmelcher, P. & Diakonos, F. K. [1998] "General approach to the localization of unstable periodic orbits in chaotic dynamical systems," *Phys. Rev.* **E57**, 2739–2746.

Schmelcher, P., Diakonos, F. K. & Biham, O. [1998] "Systematic computation of the least unstable periodic orbits in chaotic attractors," *Phys. Rev. Lett.* **81**, 4349–4352.

Shenoi, K. [1995] *Digital Signal Processing in Telecommunications* (Prentice Hall PTR, NJ).

Smale, S. [1967] "Didifferentiable dynamics systems," *Bull. Amer. Math. Soc.* **73**, 747–817.

So, P., Ott, E., Schiff, S. J., Kaplan, D. T., Sauer, T. D. & Grebogi, C. [1996] "Detecting unstable periodic orbits in chaotic experimental data," *Phys. Rev. Lett.* **76**, 4705–4708.

So, P., Ott, E., Sauer, T. D., Gluckman, B. J., Grebogi, C. & Schiff, S. J. [1997] "Extracting unstable periodic orbits from chaotic time series data," *Phys. Rev.* **E55**, 5398–5417.

Stolovitzky, G., Kaper, T. J. & Sirovich, L. [1995] "A simple model of chaotic advection and scattering," *Chaos* **5**, 671–686.

Takens, F. [1981] "Detecting strange attractors in fluid turbulence," *Dynamical Systems and Turbulence* (*Lecture Notes in Mathematics*), eds. Rand, D. & Young, L. S. (Springer-Verlag, Berlin), pp. 366–381.

Tél, T. [1990] "Transient chaos," *Directions in Chaos* (*3*)*: Experimental Study and Characterization of Chaos*, ed. Hao, B.-L. (World Scientific, Singapore), pp. 149–211.

Tél, T. & Ott, E. [1993] "Focus issues on chaotic scattering," *Chaos* **3**, 417–706.

Tél, T. [1996] "Transient chaos: A type of metastable state," *STATPHYS 19: The Proc. 19th IUPAP Conf. Statistical Physics*, ed. Hao, B.-L. (World Scientific, Singapore), pp. 346–362.

Theiler, J. [1986] "Spurious dimension from correlation algorithms applied to limited time series data," *Phys. Rev.* **A34**, 2427–2432.

Toroczkai, Z., Károlyi, G., Péntek, A., Tél, T. & Grebogi, C. [1998] "Advection of active particles in open chaotic flows," *Phys. Rev. Lett.* **80**, 500–503.

Wolf, A., Swift, J. B., Swinney, H. L. & Vastano, J. A. [1985] "Determining Lyapunov exponents from a time series," *Physica* **D16**, 285–317.

Yalcinkaya, T. & Lai, Y.-C. [1997] "Phase characterization of chaos," *Phys. Rev. Lett.* **79**, 3787–3790.

Yalcinkaya, T. [1998] *Phase Characterization of Chaos and Controlling Transient Chaos in Deterministic Flows*, Ph.D. Thesis (under Y.-C. Lai), University of Kansas.

Young, W. R. & Jones, S. W. [1991] "Shear dispersion," *Phys. Fluids* **A3**, 1087–1101.

Ziemniak, E., Jung, C. & Tél, T. [1994] "Tracer dynamics in open hydrodynamical flows as chaotic scattering," *Physica* **D76**, 123–146.

Zoldi, S. M. & Greenside, H. S. [1998] "Spatially localized unstable periodic orbits of a high-dimensional chaotic system," *Phys. Rev.* **E57**, R2511–R2514.